Chapter 3
New low-mass stars and brown dwarfs in the α Per cluster

Chapter 2 focused on the search for low-mass stars and brown dwarfs in the solar neighbourhood. Although nearby and generally amenable to detailed studies, large uncertainties remain concerning their mass estimates due to the poor age determination and the lack of trigonometric parallaxes. Therefore, the determination of the local IMF down into the substellar regime is hampered by several issues given below:

1. Accurate distance measurements are required to infer masses. However, the sample of stars with trigonometric parallaxes from the astrometric satellite *Hipparcos* is complete down to $V \lesssim 8$. A small number of fainter nearby objects have well-determined distances as well but the sample is by far incomplete. A large programme has been recently initiated in order to provide trigonometric parallaxes for objects straddling the stellar/substellar limit (Dahn et al. 2002). This survey is essential for improving the galactic field star luminosity function in the low-mass and brown dwarf regimes.

2. Nearby objects span a wide range in age from few millions years for co-moving groups and young associations to billions of years for the coolest and oldest neighbours.

3. High-mass stars are rare and almost inexistent in the solar neighbourhood due to their short lifetimes.

4. Numerous low-mass stars and brown dwarfs have now been detected in the solar vicinity over the last past years. However, their faintness renders their detection difficult as they cool off with age. Hence, the number density of low-mass stars and brown dwarfs is expected to be largely incomplete as emphasised by Henry et al. (1997).

The determination of a meaningful IMF for galactic field stars requires a volume-limited sample of objects with known age and spectral types over a large mass range. However, the incompleteness is approximately 30 % within 5 pc and double within 8 pc (Henry et al. 1997). The recent discovery of the ε Indi Ba/Bb system (Scholz et al. 2003; McCaughrean et al. 2004) at 3.626 pc provide a striking example.

To alleviate some of the issues mentioned above, many recent surveys have concentrated on young open clusters (30–200 Myr) to unearth very-low-mass stars and brown dwarfs. Indeed, open stellar clusters are good places for such quest as they represent equidistant and coeval populations of stars of similar chemical composition within a relatively small volume of space. Some caveats nevertheless remain, including the dearth of high-mass stars and issues regarding the incompleteness towards low-mass stars caused by the contamination by background objects. The best targets

are, hence, the youngest open clusters. However, *only* four open clusters are within 200 pc and younger than 200 Myr. A brief description of each cluster is given below:

- The Pleiades ($\alpha = 03°46.6^m$, $\delta = -24°4'$) is, by far, the best studied open cluster for low-mass stars and brown dwarfs. The cluster is rich (about 1200 members), nearby (~ 130 pc), young (~ 120 Myr), relatively compact, located at high galactic latitude (b = $-24°$) with a metallicity estimated to be solar (Boesgaard & Friel 1990). The extinction is low ($A_V = 0.12$ mag) and generally uniform. The large proper motion ($\mu_\alpha \cos\delta \sim +25$ mas/yr and $\mu_\delta \sim -45$ mas/yr) allows membership assessment of photometrically-selected candidates over a time scale of few years (Moraux et al. 2001). Many proper motion and photometric surveys have focused on the Pleiades, yielding the discovery of the first young brown dwarf, Teide 1 (Rebolo et al. 1995). Since that time, many brown dwarf candidates have been proposed and some confirmed spectroscopically (Martín et al. 1996; Stauffer et al. 1998). The cluster mass function over a large mass range (10–$30 M_\odot$) was well approximated by a lognormal distribution of index 1.7 and a peak around $0.25 M_\odot$ (Chabrier 2003).

- IC2391 ($\alpha = 08°40.2^m$, $\delta = -53°04'$) is a close (~ 150 pc) and young (~ 30 Myr) open cluster with solar metallicity (Randich et al. 2001). The extinction towards the cluster is rather low (E(B–V) = 0.06). Except for the brightest components of the cluster ($V \leq 11$), proper motion studies are hampered by the lack of bright members and the low galactic latitude of the cluster (b = $-6.9°$). Most of the cluster members (about 100 members) have been selected in X-rays with the *ROSAT* satellite (Patten & Pavlovsky 1999) and their membership assessed with optical photometry and/or spectroscopy (Stauffer et al. 1989a). The estimated age of 30 Myr, derived from the upper main-sequence turn-off fitting, was recently revised to 53 ± 5 Myr from the lithium test (Barrado y Navascués et al. 1999). The lithium depletion boundary was found at R–$I = 1.91$ and M(I) = 10.25 mag, corresponding to a mass of $\sim 0.12 M_\odot$, assuming a distance modulus of 5.95 and an age of 53 Myr. New brown dwarf candidates have also been extracted from a deep R and I-band survey with infrared follow-up (Barrado y Navascués et al. 2001) but no cluster mass function has been derived to date.

- IC2602 ($\alpha = 10°43^m$, $\delta = -64°24'$) is similar to IC2391 in terms of distance (d = 150 pc), age (30 Myr), and metallicity. The cluster is located around the B0Vp star θ Carinae (b = $-4.9°$) in a region of low extinction (E(B–V) = 0.04). The proper motion of the cluster is estimated to $\mu_\alpha \cos\delta \sim -9$ mas/yr and $\mu_\delta \sim +3.5$ mas/yr. This is the least studied cluster among the four cluster within 200 pc and younger than 200 Myr. The largest membership list (about 100 members) was established by Randich et al. (1995) through an X-ray study conducted with the *ROSAT* satellite. Photometric and spectroscopic follow-up confirmed most candidates as genuine cluster members (Prosser et al. 1996a). No cluster mass function is available at present.

- The α Per cluster ($\alpha = 03°50^m$, $\delta = 49°00'$) has been well studied, though less than the Pleiades due to its smaller proper motion ($\mu_\alpha \cos\delta \sim +23$ mas/yr and $\mu_\delta \sim -25$ mas/yr) and lower galactic latitude (b = $-7°$). The cluster is located north-east of the F5V supergiant Alpha Persei at a distance of about 180 pc and solar metallicity (Boesgaard & Friel 1990). The extinction towards the cluster was estimated to be $A_V = 0.30$ mag with possible spatial variations. Several proper motions, photometric and spectroscopic surveys have

revealed about 400 members in α Per (Prosser 1994). The cluster was also extensively studied in the X-rays, yielding new member candidates based on *ROSAT* observations (Randich et al. 1996; Prosser et al. 1996b). The lithium test applied to the cluster yielded an age of 90 ± 10 Myr (Stauffer et al. 1999). The cluster mass function is well approximated by a power law with an index $\alpha = 0.59 \pm 0.05$ in the 0.30–0.035 $M_\odot$ mass range (Barrado y Navascués et al. 2002). We will provide more details about those surveys in the next sections ($\S$ 3.1–3.4) and emphasise our contribution to the α Per cluster in $\S$ 3.5 and $\S$ 3.6.

The present chapter is dedicated to a comprehensive study of the young open cluster α Per carried out within the framework of our collaboration. The α Per cluster is richer than IC2391 and IC2602 but probably less rich than the Pleiades. The cluster presently has about 400 catalogued members compared to about 1200 for the Pleiades. However, the cluster member list of α Per is much less complete than the Pleiades for three major reasons:

1. The number of deep optical and/or proper motion surveys implemented in α Per is smaller than in the Pleiades.

2. The cluster mean proper motion is not well separated from field stars.

3. α Per is located at lower galactic latitude than the Pleiades.

This chapter is organised as follows. In $\S$ 3.2, we review results from surveys dedicated to the search for low-mass cluster members in α Per. In $\S$ 3.2, we report the recent determination of the age of the cluster by the "lithium test" (Stauffer et al. 1999). In $\S$ 3.3, we describe the main results of the optical wide-field survey in the α Per cluster carried out within our collaboration (Barrado y Navascués et al. 2002), including the determination of the luminosity function ($\S$ 3.4.1) and the mass function ($\S$ 3.4.2). In $\S$ 3.5, we describe the selection of new cluster member candidates including new brown dwarfs from a near-infrared survey of a 0.70 square degree area in the cluster. Optical spectroscopic follow-up of a subsample of selected cluster member candidates is presented in $\S$ 3.6. We compare the updated α Per mass function to the field and Pleiades-like open clusters in $\S$ 3.7. Conclusions and future work are discussed in $\S$ 3.8.

The results presented in this chapter have been (or will be) published in several papers, including:

1. Barrado y Navascués, Bouvier, Stauffer, Lodieu, & McCaughrean (2002) where I have provided infrared photometry of faint optically-selected cluster members.

2. Lodieu, McCaughrean, Bouvier, Barrado y Navascués, & Stauffer (2003) published the major results of the near-infrared wide-field survey described in $\S$ 3.5 in the IAU211 conference proceedings.

3. The new results related to the near-infrared wide-field survey will be part of a forthcoming paper (Lodieu et al. 2004, in preparation). This part of the work has been essentially done by myself.
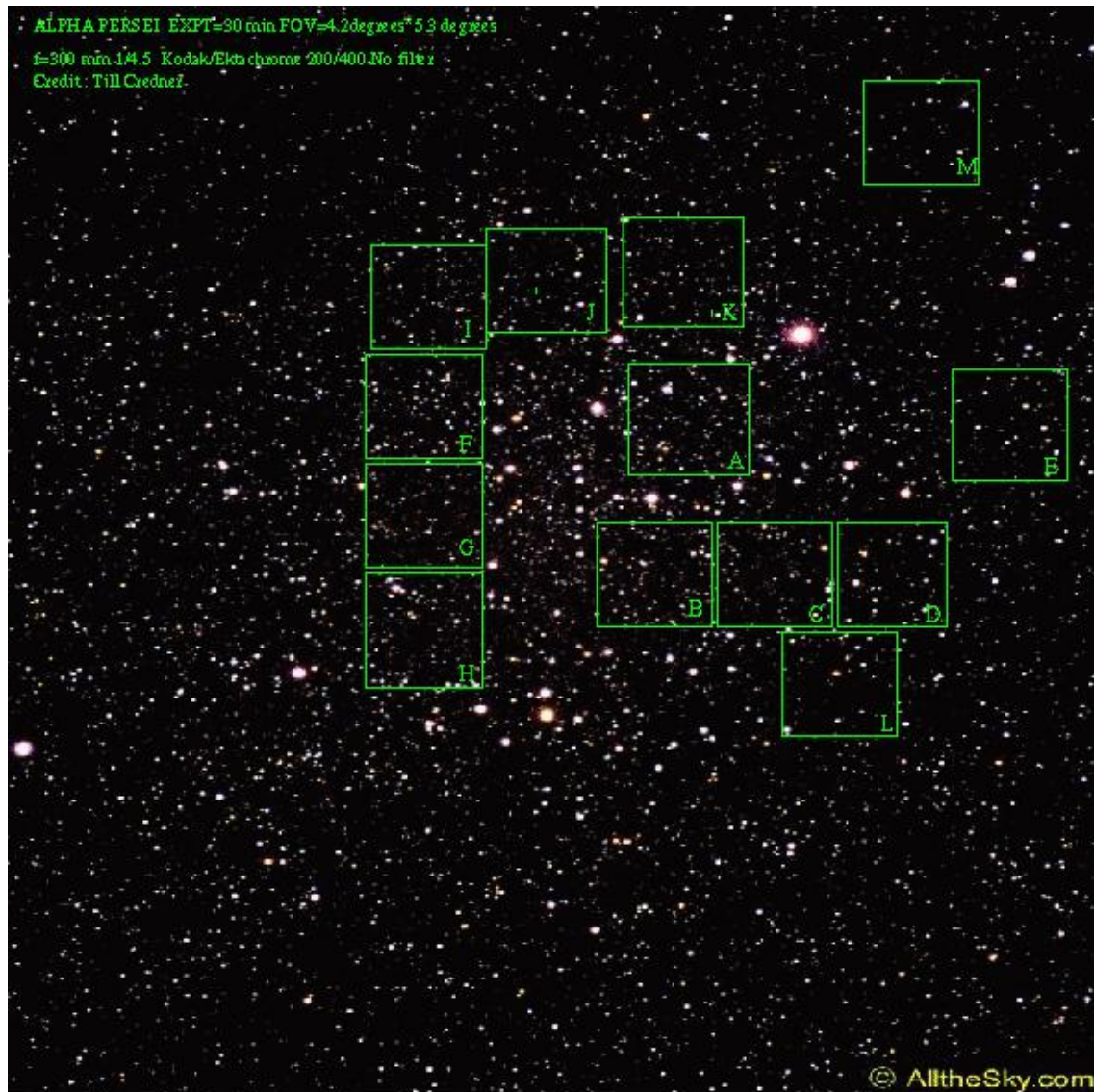
Figure 3.1: Image of a $4.2° \times 5.3°$ towards the α Per cluster. North is at the top and East to the left. A concentration of stars is seen south-east of the brightest star in the image, the F5 supergiant Alpha Persei. The green squares represent the 13 KPNO/MOSA fields-of-view ($35.4' \times 35.4'$) observed in the R_c and I_c bands down to a completeness limit of 21.9 and 20.75, respectively. *Copyright: T. Credner & S. Kohle, AlltheSky.com*

3.1   Known members of the α Per cluster

The α Per cluster is clearly seen on photographic plates as a concentration of stars south-east of the F5 supergiant Alpha Persei, whose membership of the cluster is estimated to 97 % probability (de Zeeuw et al. 1999). Figure 3.1 is a $4.2° \times 5.3°$ image taken towards the α Per cluster.

Several authors, including Heckmann, Stauffer, Prosser and collaborators, have extensively

studied the bright components and low-mass members of the α Per cluster. The membership assessment made use of proper motion, multi-band photometry, optical spectroscopy for Hα and lithium detection, as well as radial and rotational velocities. We will briefly summarise previous surveys designed to identify low-mass members in the α Per cluster.

1. Heckmann, Dieckvoss, & Kox (1956) obtained proper motions for stars brighter than a V magnitude of 12.0 in the vicinity of α Per. Slightly more than 10 % of the 1400 stars surveyed within the field-of-view were identified as probable cluster members. Those members were termed by HE (as Heckmann) followed by three digits starting with one. *UBV* photometry of those ~ 150 new members was obtained by Mitchell (1960), providing reddening and distance estimates as well as criteria to reject non members.

2. Stauffer et al. (1985) surveyed a $1.2° \times 1.2°$ area of the α Per cluster and obtained proper motion for 4000 stars down to $V \sim 16.0$ mag. Proper motion, *VRI* photometry, Hα emission, radial and rotational velocities were used as main criteria to select about 90 new low-mass cluster members. Those new G, K, and M cluster dwarfs with high rotational velocities roughly span the 0.5–$1.2 \, \mathrm{M_\odot}$ mass range, assuming a distance of 165 pc and an age of 50 Myr. These objects were termed by AP as in 'Alpha Per' followed by three digits starting with one.

3. Stauffer, Hartmann, & Jones (1989b) identified new low-mass members over a 2.5 square degree region in α Per based on proper motion, *BVRI* photometry, and subsequent spectroscopy. The percentage of cluster members compared to the total number of stars along the line of sight drops to few percents from $V = 10$ to $V = 15$ mag due to the low galactic latitude of α Per. In total, Stauffer et al. (1985, 1989b) confirmed the membership of 30 HE members and 50 AP stars and identified new members down to $V \sim 16.0$ mag.

4. Prosser (1992) carried out an extensive membership survey of a $6° \times 6°$ whole Palomar photographic plate in the α Per cluster. About 130 new cluster members among a sample of proper motion candidates were extracted down to $V \sim 19.0$ mag, using additional photometric and spectroscopic information. Spectral types were also provided for some candidates brighter than $V = 17$ mag, corresponding to a spectral type of M4. The spatial distribution of the new members (filled circles) is shown in Figure 3.2. This study provided a revised age for the cluster to 80 Myr based on isochrone fitting with no significant age spread. The mean reddening was estimated to E(V–I) = 0.18, consistent with previous determinations although some spatial variations across the cluster were reported.

5. In an attempt to search for low-mass members in the α Per cluster, Prosser (1994) obtained new CCD images of a ~ 0.8 square degree area in the cluster in the V and I bands down to $V \sim 22.0$ mag. Contrary to former surveys, no first epoch was available at these faint magnitudes. About new 30 new cluster member candidates were solely selected on the basis of their location in the (V, V–I) colour-magnitude diagram. Low-dispersion spectroscopy obtained for some of the new candidates, confirming the cluster membership of eight objects and classified three others as non-members.

6. A raster scan and pointed X-ray observations were obtained towards the α Per cluster with the *ROSAT* satellite in the soft (0.1–0.4 keV) and hard (0.4–2.0 keV) bands.

The raster scan covered $\sim 10 \deg^2$ in α Per with an exposure time of 10 ksec, yielding limiting sensitivity of $L_X \sim 10^{29}$ erg sec^{-1} (Randich et al. 1996). Out of ~ 160 X-ray detections, 89 were associated with previously selected cluster members. More than 80 % of the F, G, and K dwarfs and ~ 50 % of the M dwarfs belonging to the cluster were detected.

The *ROSAT* pointing observations (Prosser et al. 1996b), exposed 22–25 ksec, covered a slightly smaller area (three pointings ~ 50 arcmin in radius) than the raster scan but achieved higher sensitivities. About 80 X-ray sources, including 40 common to the raster scan, were associated with an optical counterpart from previous proper motion surveys. All the K dwarfs and a high number of M dwarfs belonging to the cluster were detected by the pointing observations. However, both surveys revealed about 200 sources with no optical counterparts. Photometry along with low- and high-dispersion spectroscopy classified about 40 X-ray sources as probable new cluster members (Prosser & Randich 1998; Prosser et al. 1998). A detailed analysis of the X-ray properties of the F, G, K, and M cluster dwarfs detected with *ROSAT* led to the following results:

(i)   The X-ray luminosity peaks at G dwarfs and then declines towards M dwarfs, suggesting that the dynamo activity efficiency decreases towards low-mass stars.

(ii) Rotational velocities are correlated with the X-ray luminosity. Fast rotators with velocities larger than 15 km s^{-1} have larger X-ray luminosities than slow rotators.

(iii) The mean X-ray luminosity of F and G stars in α Per is larger than in their Pleiades counterparts whereas no difference is found for K and M dwarfs. This result indicates that F and G stars are spinning down faster in α Per than in the Pleiades.

Due to the low galactic latitude (b = −7°) of the α Per cluster, it was quickly recognised that proper motion and photometry alone would fail to eliminate all non-members. Radial and rotational velocities as well as spectroscopic features, including Hα in emission at 6563 Å and lithium in absorption at 6708 Å provide additional criteria suggestive of cluster membership. Hence, a full analysis of membership in α Per requires large amount of observing time as well as a variety of measurements and analysis. We will now review recent improvements achieved within the framework of our collaboration on the α Per cluster.

3.2   The age determination of the α Per cluster

The age determination of open clusters originates traditionally from isochrone fitting of the upper main-sequence and giant branch. However, this method is generally hampered by the small number of stars evolving off the main-sequence, their photometric uncertainties, their unknown binary status, and the difficulties in modelling the amount of mixing of hydrogen-rich matter into the convective core ("convective core overshoot"). Depending on the amount of overshoot (no overshoot versus strong overshoot), the age of open clusters can vary by a factor of two (Mermilliod 1981; Mazzei & Pigatto 1988).

Recently, a new method, the "lithium test" was proposed to estimate the age of open clusters (Rebolo et al. 1992). The idea is that for low-mass stars, lithium is quickly destroyed and, therefore, unobservable in their spectra. On the contrary, brown dwarfs preserve their lithium content because the central temperature is not sufficient to fuse hydrogen. The lithium depletion
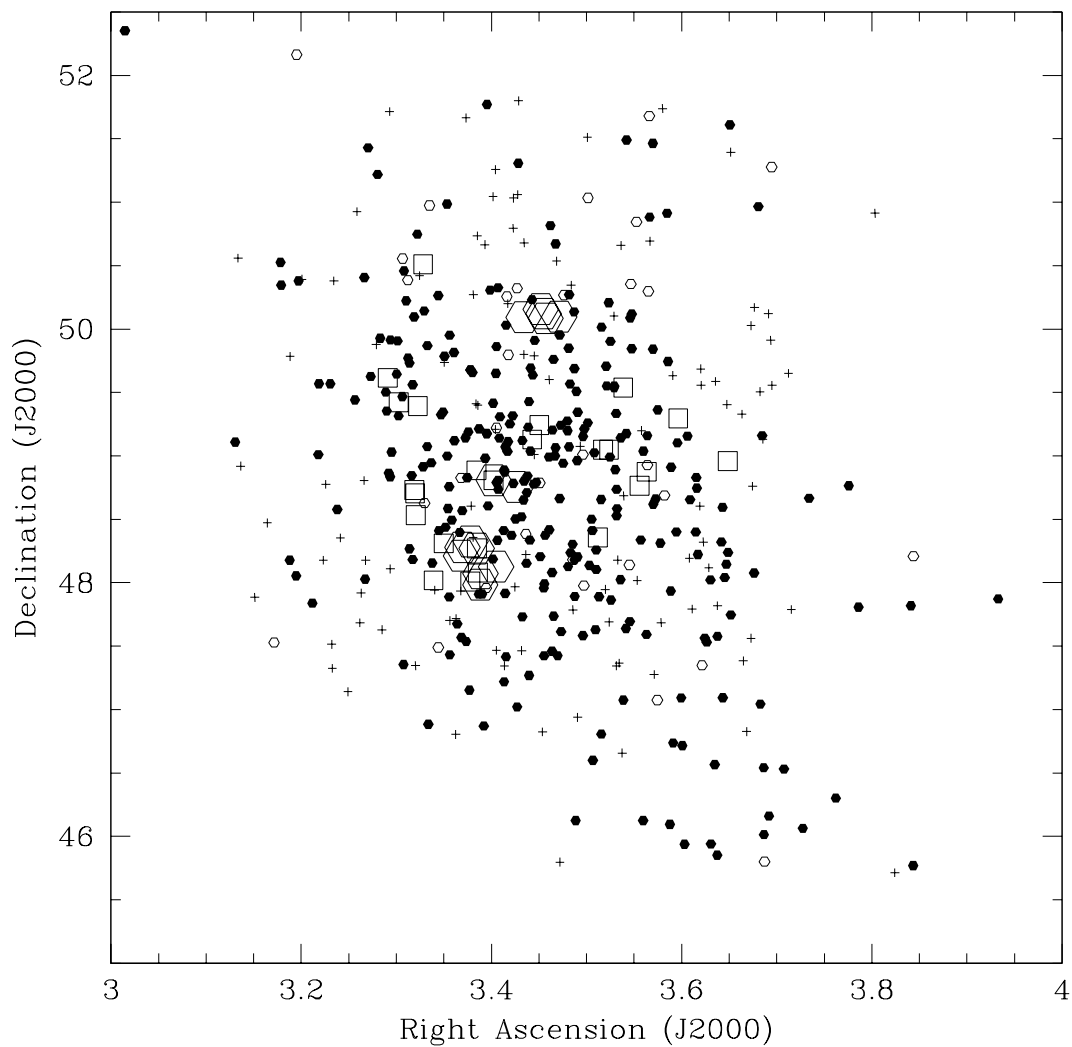
Figure 3.2: Location of known α Per members in the (ra, dec) frame. Filled circles, open circles, and crosses are the probable, possible members, and non-members, respectively, based on surveys dedicated to low-mass members in α Per. Open squares are spectroscopically confirmed cluster members from Stauffer et al. (1999). Large open hexagons are new infrared-selected candidates from our wide-field survey (Section 3.5)

boundary, the point where lithium has been depleted by a factor of 100, is expected to be sharp with no lithium for objects above the limit and cosmic abundance essentially for objects below the boundary. Furthermore, as stars are fully convective in the mass range of interest, the surface lithium abundance reflects directly the core abundance, yielding smaller uncertainties than the "convective core overshoot" determination. The mixing theory in the atmospheres of low-mass stars remains none the less poorly constrained. Applied successfully to the Pleiades, the value of

the age increased by a factor of two from 70 Myr to 125 Myr (Stauffer et al. 1998). A similar result holds for the young open cluster IC 2391 with an age of 35 Myr derived from upper main-sequence fitting and 53 Myr inferred from the lithium test (Barrado y Navascués et al. 1999).

The lithium test was recently applied to the α Per cluster based on a $6\,\text{deg}^2$ optical survey in the R_c and I_c broad-band filters (Stauffer et al. 1999). A few bona-fide cluster member candidates were identified in a limited magnitude range ($16.25 \leq I \leq 18.75$) to seek for lithium absorption at $6708\,\text{Å}$ and subsequently infer the lithium depletion boundary. The selection procedure yielded 27 bona-fide member candidates redder than the Zero-Age Main Sequence (hereafter ZAMS; Leggett 1992), shifted to the distance of the cluster ($d = 176\,\text{pc}$; Pinsonneault et al. 1998) in the (I_c,R_c–I_c) colour-magnitude diagram. The bad agreement between the theoretical isochrones and the sequence of cluster members originates from the difference between the ZAMS of old field dwarfs and the isochrones drawn for pre-main-sequence stars. In addition, models do not predict accurate optical colours due to the incompleteness of the current opacity line lists. Low- and high-resolution spectroscopy were carried out with the Low-Resolution Imaging Spectrograph (LRIS) on Keck II telescope for 14 and 11 candidates, respectively. Among the probable and possible member candidates, five objects did exhibit lithium in absorption whereas nine others did not, yielding a sharp determination in (R_c–I_c) colour and more uncertain value of the I_c magnitude.

Table 3.1: Field centres observed in the α Per cluster with CCD Mosaic Imager on the KPNO-4m telescope. Each image has a $35.4' \times 35.4'$ field-of-view with a spatial scale of $0.26''$. Right ascension and declination are given in J2000. The five optical fields followed-up in the K'-band using Omega-Prime on the Calar Alto 3.5-m telescope are indicated with the respective observing dates, exposure times, surveyed area, and limiting magnitudes. I observed fields E, K, and L in the near-infrared whereas Thomas Stanke observed the A and C fields.

Field	R.A.	DEC	Near-infrared follow-up			
	(J2000.0)		Obs. Date	ExpT	Area	K'_{lim}
A	03:27:10.00	49:24:00.0	04–06 Dec 98	20 min	$580'^2$	17.5
B	03:28:00.00	48:42:00.0				
C	03:24:50.00	48:42:00.0	06 Dec 98	20 min	$280'^2$	17.5
D	03:21:40.00	48:42:00.0				
E	03:19:35.00	49:27:00.0	14 Dec 00	20 min	$560'^2$	15.5
F	03:33:45.00	49:35:00.0				
G	03:33:45.00	49:04:00.0				
H	03:33:45.00	48:34:00.0				
I	03:33:45.00	50:06:00.0				
J	03:30:30.00	50:09:00.0				
K	03:27:00.00	50:13:00.0	11–12 Dec 00	20 min	$560'^2$	17.5
L	03:23:10.00	48:11:00.0	11–12 Dec 00	20 min	$560'^2$	17.5
M	03:21:00.00	50:48:00.0				

The adopted values for the lithium depletion boundary were R_c–$I_c = 2.12$ and $I_c = 17.70 \pm 0.15$ mag. Assuming a distance modulus of 6.23, and applying the NextGen isochrones from Baraffe et al. (1998), Stauffer et al. (1999) derived an age of $90 \pm 10\,\text{Myr}$ for α Per, twice larger than the

50 Myr value from the turn-off main-sequence fitting. The lithium depletion boundary based on the K-band photometry was estimated to be at $M_K \sim 8.3$ mag and $(I_c - K) \sim 3.07$, though with larger uncertainties. Note that comparison with other evolutionary tracks (D'Antona & Mazzitelli 1994; Burrows et al. 1997) led to similar values of the age within the uncertainties. **We will adopt the age of 90 ± 10 Myr for subsequent analysis of the α Per cluster unless otherwise stated**. We note that Basri & Martín (1999b) derived an age age between 65 and 75 Myr from the detection of the lithium absorption line in a handful of objects.

3.3 The wide-field optical survey of the α Per cluster

The aim of Stauffer et al. (1999) was to locate the lithium depletion boundary in α Per to derive the cluster age. No attempt was made to select a complete sample of low-mass stars and brown dwarf member candidates and derive the cluster mass function. Nevertheless, Stauffer et al. (1999) obtained spectroscopy for a subsample of objects, including two brown dwarf candidates.

Meanwhile, a new wide-field optical survey was conducted with the KPNO/MOSA detector and covered ~ 4.5 square degrees in the α Per cluster to unearth new low-mass stars and brown dwarfs over the largest possible area in the cluster. The MOSA (Mosaic Imager) detector mounted on the Kitt Peak 4-m telescope is a 8192×8192 pixels CCD array with a spatial scale of $0.26''$/pixel, yielding a $35.4' \times 35.4'$ field-of-view. Thirteen fields-of-view (see Table 3.1 and Figure 3.1 for coordinates and locations in the cluster) were observed, reaching detection and completeness limits of $R_c \sim 25.5$ and 21.9 mag, and $I_c \sim 22.5$ and 20.75 mag, respectively (Barrado y Navascués et al. 2002).

A sample of 94 cluster member candidates was extracted from 260 000 detections in the 4.5 deg^2 surveyed area based on their location in the optical $(I_c, R_c - I_c)$ colour-magnitude diagram (Figure 3.3). All objects located to the right of the empirical Zero-Age Main-Sequence (Leggett 1992) shifted to the distance of α Per were classified as candidate cluster members. The gap between field stars and cluster candidates is detectable (Figure 3.3) although not as sharp as in the Pleiades (Bouvier et al. 1998). Indeed, a higher contamination by field stars and background giants is expected, as α Per is located at lower galactic latitude than the Pleiades (b $= -7°$ versus b $= -24°$).

To estimate the contamination by field stars, Barrado y Navascués et al. (2002) obtained near-infrared photometry in the K'-band for most of the optically-selected candidates, in the J-band for 24 of them, and in the H-band for a handful of objects, using Omega-Prime and Omega-Cass cameras on the 3.5-m telescope and the MAGIC camera on the 2.2-m telescope at Calar Alto. The membership status of the optically-selected cluster member candidates was assessed by comparing the location of the objects to the NextGen (Baraffe et al. 1998), Dusty, and Cond (Chabrier et al. 2000b) isochrones in various colour-magnitude diagrams. Objects located to the right of the isochrones in all the diagrams were classified as probable members whereas those to the left were rejected as cluster members. The candidates were classified as follows:

- 54 ($\sim 60\%$) as probable members

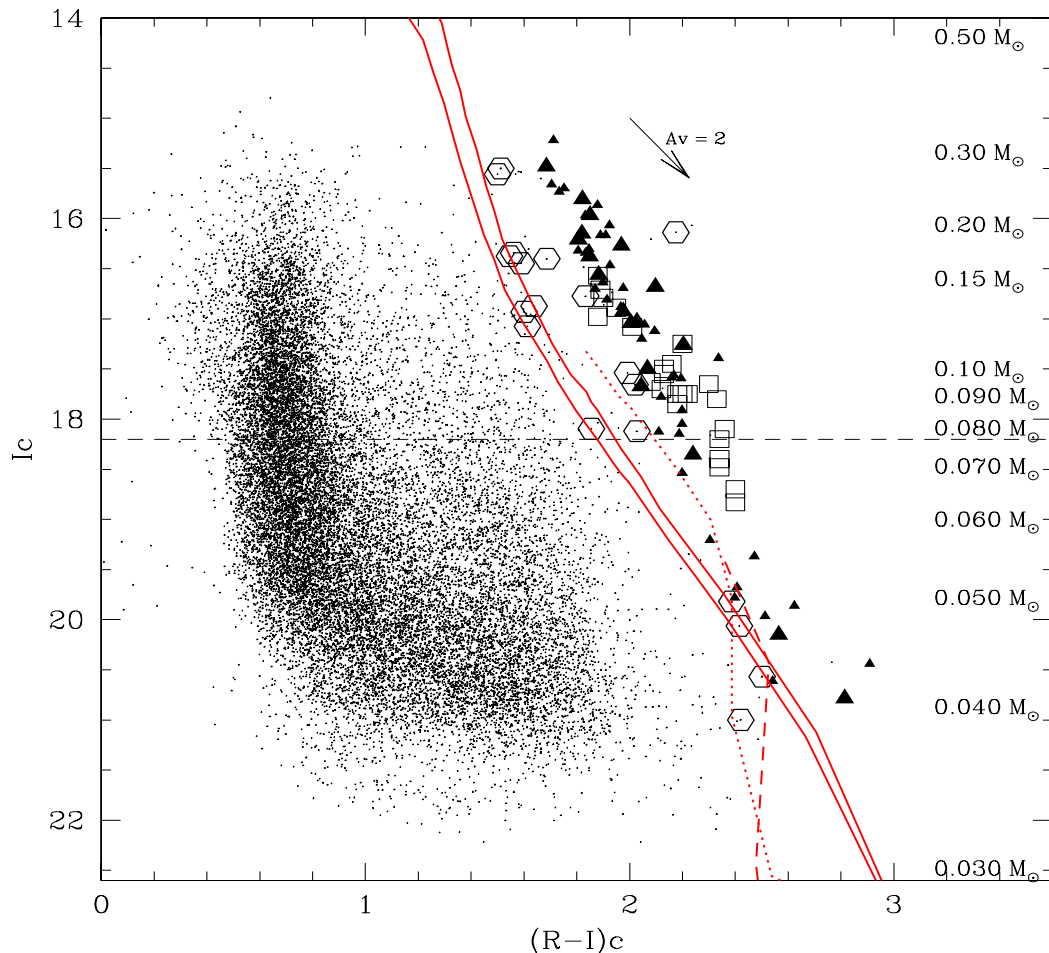- 12 ($\sim 12\%$) as possible members

- 26 ($\sim 28\%$) as non-members

Figure 3.3: Colour-magnitude (I_c, I_c–R_c) for all optical detections within the 0.70 square degree area followed-up in the near-infrared with the Omega-Prime camera. Large filled triangles are probable candidates from Barrado y Navascués et al. (2002) recovered in our optical-infrared selection whereas small filled triangles were not recovered. Open hexagons are the new infrared-selected cluster member candidates. Large open hexagons indicate the new candidates to the right of the NextGen 100 Myr isochrones in the optical-to-infrared colour-magnitude diagram. Open squares are spectroscopically confirmed cluster members from Stauffer et al. (1999). Also overplotted are the NextGen (Baraffe et al. 1998) isochrones for 50 and 100 Myr (solid lines), the Cond (dotted line) and Dusty (dashed line) 100 Myr isochrones (Chabrier et al. 2000b), assuming a distance of 182 pc. A reddening vector for $A_V = 2$ is also included for comparison purpose. The horizontal dashed line at $I_c = 18.2$ indicates the stellar/substellar boundary at 0.075 $M_⊙$, assuming a distance of 182 pc and an age of 90 Myr for the cluster (Stauffer et al. 1999). The mass scale is indicated on the right side of the plot. The discrepancy between isochrones and cluster candidates might originate from the uncertainties on the current opacity line lists.

Thus, the contamination by field stars lies in the range 28–40 %, estimate slightly larger than in the Pleiades (Bouvier et al. 1998; Martín et al. 2000a; Moraux et al. 2001). Based on this sample of approximately 100 objects, Barrado y Navascués et al. (2002) derived luminosity and mass functions for α Per in the 0.30–0.05 $M_\odot$ mass range. The influence of the contamination and the age on the shape of the mass function was analysed as well.

3.4 The luminosity and mass functions of the α Per cluster

3.4.1 The cluster luminosity function

Barrado y Navascués et al. (2002) derived the luminosity function for very low-mass stars and brown dwarfs in α Per according to the sample of probable and possible cluster members (dashed line with filled circles in Figure 3.4). The completeness and detection limits of $I_c = 19.5$ and 22.5 mag translate into masses of 0.050 $M_\odot$ and 0.035 $M_\odot$, respectively, assuming a distance of 176 pc and an age of 90 Myr for the α Per cluster. The luminosity function is displayed in Figure 3.4. The solid and dashed lines with filled circles show the cluster luminosity function before and after rejection of non-members, respectively. The solid line with open circles represent the number of stars per magnitude bin for a sample of field stars with an arbitrary shift of -0.2 mag in the R–I colour compared to cluster members.
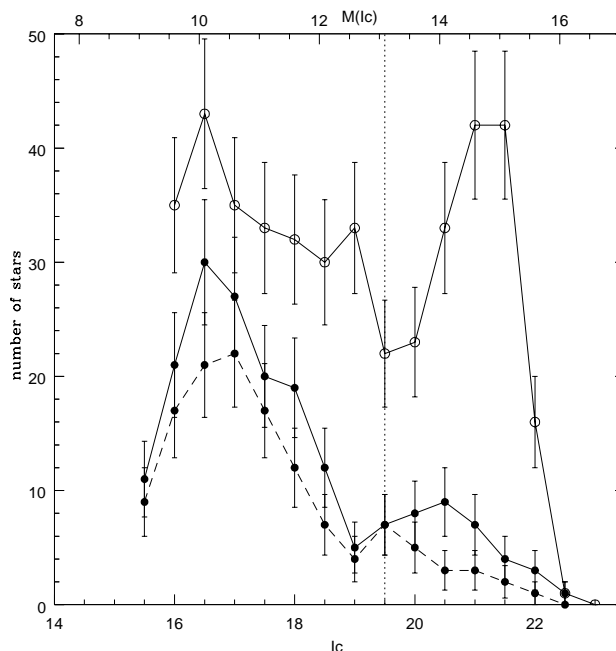

Figure 3.4: Luminosity function (number of stars per bin of magnitudes) of the α Per cluster before and after rejecting the non-members (solid and dashed line with filled circles, respectively). The distance modulus is 6.22, corresponding to a distance of 176 pc. Apparent and absolute magnitudes are plotted on the lower and upper abscissae, respectively. The upper solid line with open circles was derived for a comparison sample of field stars. From Barrado y Navascués et al. (2002).

Compared to a control field luminosity function, the cluster luminosity function (Figure 3.4) exhibits several features detailed below:

1. A peak at $M_I = 10$, detected in the luminosity function of the control field and in other open clusters, including the Pleiades (Zapatero Osorio et al. 1997c). This peak was, however, located at $M_I = 11$ mag in NGC 2516 (Jeffries et al. 2001) and at $M_I = 9$ mag in M35 (Barrado y Navascués et al. 2001), suggesting that the location of this feature is not universal in clusters 100–200 Myr old and might be age dependent. This maximum might correspond to the H_2-convection peak identified by (Kroupa et al. 1990, 1993) in the luminosity function of nearby field stars.

2. A gap was detected at $M_I \sim 12.5$ mag, corresponding to $0.055\,M_\odot$ and spectral types ranging from M6 to M8. This feature was already apparent at same spectral type in other clusters at different ages, including σ Orionis (Béjar et al. 2001), the Trapezium Cluster (Lucas & Roche 2000), IC348 (Luhman 1999), the Pleiades (Jameson et al. 2002), and IC 2391 (Barrado y Navascués et al. 2001a). Jameson et al. (2002) suggested that the formation of large dust grains at those specific temperatures could be responsible for this feature although it might result from the formation mechanism of low-mass objects.

3. A second peak at $M_I = 14.5$ mag was detected in the cluster luminosity function but not in the control field. This feature was, however, below the completeness limit of the survey and should be interpreted with caution.

3.4.2   The cluster mass function

Barrado y Navascués et al. (2002) transformed the α Per luminosity function into a cluster mass function (Figure 3.5 using the NextGen models from Baraffe et al. (1998). The conversion of the luminosity function into a mass function requires a mass-magnitude relation extracted from evolutionary tracks. The choice of a particular set of isochrones had, however, little influence on the shape and the slope of the mass function (Barrado y Navascués et al. 2002). The influence of the age on the mass function was studied as well: no variation on the slope and the shape of the cluster mass function was obvious (Barrado y Navascués et al. 2002). Varying the age shifts only the mass of the objects towards higher and lower masses when older and younger, respectively. Moreover, the cluster mass function derived with the different kind of membership selection criteria exhibits little difference as shown in Figure 3.5. The influence of binaries on the shape and the slope of the mass function is not considered in this study although it can affect the power law index by up to 0.5 (Kroupa 2001).

The most probable mass function in the α Per cluster is displayed as a thick solid line in Figure 3.5. Two estimates of the Pleiades mass function from Bouvier et al. (1998; $\alpha = 0.56$) and Zapatero Osorio (2002, personal communication; $\alpha = 0.75$) are displayed in Figure 3.5 as well. The slope of the α Per mass function in the 0.30–$0.035\,M_\odot$ mass range was approximated by a power law with an index $\alpha = 0.59 \pm 0.05$ for comparison with other mass function estimates in open clusters (Barrado y Navascués et al. 2002). The shape of the mass function might, however, reflect some physics intrinsic to stars. A drop is detected at $0.055\,M_\odot$ in the cluster mass function. A second drop at $0.035\,M_\odot$ is also detected but is uncertain as it is located below the completeness limit of the survey.
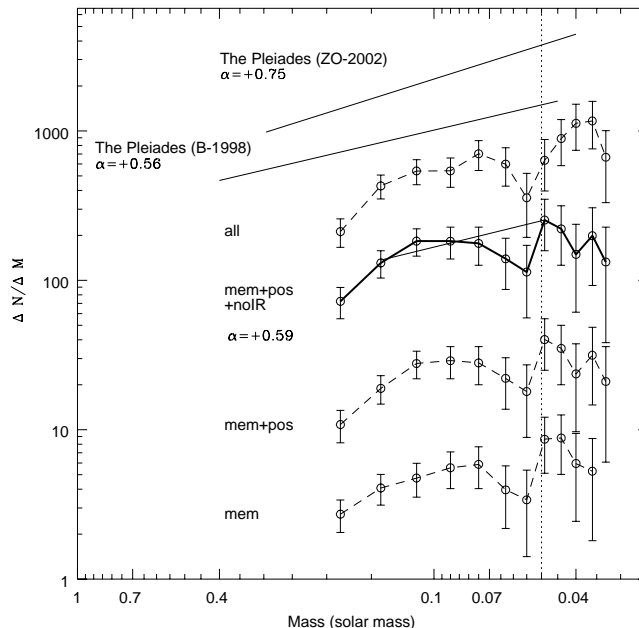
Figure 3.5: Mass functions of the α Per cluster, illustrating the effect of contamination by field stars. These mass functions were derived using a 80 Myr isochrone (Baraffe et al. 1998). From top to bottom, mass functions are displayed for all members, all members except the non-members, probable and possible members, and finally for only probable members. The most probable mass function is shown as a thick line. A linear fit to this mass function is also included, with a power law index of $\alpha = 0.59 \pm 0.05$ when expressed as a power spectrum. For comparison, the Pleiades mass function, by Bouvier et al. (1998), valid between 0.40 and 0.045 $M_\odot$, and by Zapatero Osorio (2002, personal communication), derived in the 0.3–0.040 $M_\odot$ mass range are included. Figure taken from Barrado y Navascués et al. (2002).

In summary, **the α Per mass function (Figure 3.5) is similar to the various estimates of the Pleiades mass function over the same mass range** (Bouvier et al. 1998 inferred $\alpha = 0.6$; Dobbie et al. 2002 derived $\alpha = 0.8$; and Tej et al. 2002 found $\alpha = 0.5$).

3.5 The near-infrared survey of the α Per cluster

The main purpose of the K'-band follow-up survey was to detect new cluster member candidates, including lower mass brown dwarfs down to the deuterium burning limit around 0.013 $M_\odot$ when combined with the wide-field optical observations presented in § 3.3.

We present in this section a near-infrared (K'-band) survey of 0.70 square degree area in the α Per open cluster conducted with the Omega-Prime camera mounted on the Calar Alto 3.5-m telescope. The completeness limit of the near-infrared survey is deep enough to probe the substellar regime down to the deuterium burning limit. According to the Dusty isochrones from Baraffe et al. (1998), a 20 $M_{\rm Jup}$ object in the α Per cluster has a ($I–K$) colour of about 9.0 and

$K = 18.1$, assuming an age of 90 Myr and a distance of 182 pc. We have chosen a compromise for the cluster distance between the *Hipparcos* estimate (d = 190 pc; Robichon et al. 1999) and the main-sequence fitting (d = 176 pc; Pinsonneault et al. 1998). The latter estimate was used by Barrado y Navascués et al. (2002) to infer the cluster luminosity and mass functions.

This section is structured as follows. First, the near-infrared observations carried out with Omega-Prime are presented in § 3.5.1. Second, the data reduction and the extraction of the photometry are described in § 3.5.2. Third, the astrometry of the near-infrared fields is detailed in § 3.5.3. Finally, the optical-infrared catalogue is provided in § 3.5.4 and new cluster member candidates are extracted from the colour-magnitude (§ 3.5.5) and colour-colour (§ 3.5.6) diagrams, respectively.

3.5.1 Observations

Five of the optical fields, observed in the R_c and I_c bands with the KPNO/MOSA detector (Table 3.1), were followed-up in the near-infrared (K'-band at 2.12 μm) using the wide-field camera Omega-Prime mounted on the Calar Alto 3.5-m telescope. Omega-Prime has a 1024×1024 pixel HAWAII detector with a spatial scale of $0.396''$/pixel, yielding a $6.7' \times 6.7'$ field-of-view (Bizenberger et al. 1998). At the time of the observations, Omega-Prime had the largest field-of-view among infrared detectors at Calar Alto[1]. The near-infrared observations presented in this section were carried out at two different epochs (Table 3.1) and cover a total area of 0.70 square degree in the α Per cluster. This area represents only about half of the total area covered by the five KPNO/MOSA fields-of-view despite the large field-of-view of the Omega-Prime camera.

The first set of data was obtained on 4–6 December 1998 under good seeing ($\sim 1''$) but non-photometric conditions. Mosaics of 3×3 and 4×4 Omega-Prime fields-of-view were obtained for the A and C optical fields, respectively. The second set of data was obtained two years later on 11–14 December 2000. Two 4×4 mosaics in the K and L fields were obtained during the first three nights under variable seeing (between $1''$ and $1.4''$) and non-photometric conditions. The field E was observed during the last night under poor weather conditions (and bad seeing) and is, therefore, shallower than the other fields (Table 3.1).

Twenty exposures of 1 min each dithered by less than $40''$ around the centre of each field were obtained to subtract the sky background and keep a good signal-to-noise ratio over the largest area possible. Series of five differential (lights on – off) dome flat fields were taken before and after each night of observations, as well as series of ten dark frames with exposure times similar to those of the targets. Several standard stars were selected from the near-infrared catalogue of Northern Hemisphere standard stars by Hunt et al. (1998), some stars being common to the Faint Standard catalogue (Landolt 1992) to estimate the zero-points throughout the night. A five-dither pattern was observed for each individual standard star. The observed standards were FS1, FS16 and FS17, FS23, FS31, FS32, FS33, and AS15 over the four nights with FS16 and FS17 taken on three different nights to cross-check the zero points. The centre of the K field in α Per, taken on the first night, was observed again during the remainder nights for internal calibration.

---

[1]This instrument has now been superseded by Omega2000, a $15.4' \times 15.4'$ camera with a spatial scale of $0.3''$/pixel on the Calar Alto 3.5-m telescope

3.5.2 Data reduction

The observing procedure and the data reduction method were accomplished in a similar manner for both sets of data and carried out within the IRAF environment (package *digiphot*).

- The flat-field exposures were averaged using a minmax rejection algorithm i.e. the lowest and highest values were rejected and the remainder averaged.

- Each on-source frame was sky-subtracted using the median of the remaining dithered images and divided by the averaged flat field.

- The individual images were averaged to create a 20 min-exposure image. The final images were trimmed to keep the central part with the total exposure time of 20 minutes and reject the edges with lower signal-to-noise. Due to the dithering pattern, roughly 100 pixels were trimmed in both x and y coordinates, resulting in a final 6×6 square arcmin usable field-of-view.

We adjusted the full-width-half-maximum, the sky level and the detection threshold for source detection in the field, providing (x,y) coordinates and photometry for each individual object. To optimise the photometry, we have applied an aperture similar to the FWHM to each detection. The flux of few relatively bright and isolated stars was measured for different aperture sizes (from 1 to 4 times the FWHM) to compute the aperture correction. The sky was estimated from a $3 \times$FWHM-wide annulus at a radius of $4 \times$FWHM from the centre of the star. Then, we have corrected the resulting magnitudes for extinction and zero points using the 2MASS K_s photometry available for some patches in the α Per cluster. The zero points differ for each individual Omega-Prime field-of-view caused by the non-photometric conditions and the zero-points derived from the standard stars were different at a level higher than the accuracy of 0.1 mag. No obvious colour term was seen between the K' and the K_s broad band filters.

The completeness limit of each field, defined as the magnitude where the histogram of the number of stars per bin of magnitude stops increasing, is listed in Table 3.1 and displayed in Figure 3.6. Galactic models (Annie Robin personal communication) predict a rising luminosity function up to $K \sim 21.0$ (lower right panel in Figure 3.6). Therefore, the magnitude at which the observed luminosity drops is likely the completeness limit of the survey and not a feature intrinsic of the field luminosity function as it happen three magnitudes brighter than the model predictions. A similar approach was applied by Barrado y Navascués et al. (2002) to estimate the completeness limits of the optical wide-field survey in α Per.

3.5.3 Astrometry of the near-infrared images

Accurate astrometry in the near-infrared was necessary to cross-correlated our infrared survey with the previous optical data (Barrado y Navascués et al. 2002. The astrometry of the near-infrared images was carried out with IRAF (package *imcoord* including the tasks *ccxymatch*, *ccmap*, *ccsetwcs*, and *cctran*).

The astrometry of the K'-band images was done by matching the observed K' coordinates (x,y) and the equatorial (ra,dec) coordinates from the USNO-A2 catalogue (Monet et al. 1998) for relatively bright stars located in the Omega-Prime field-of-view. The USNO-A2 catalogue was
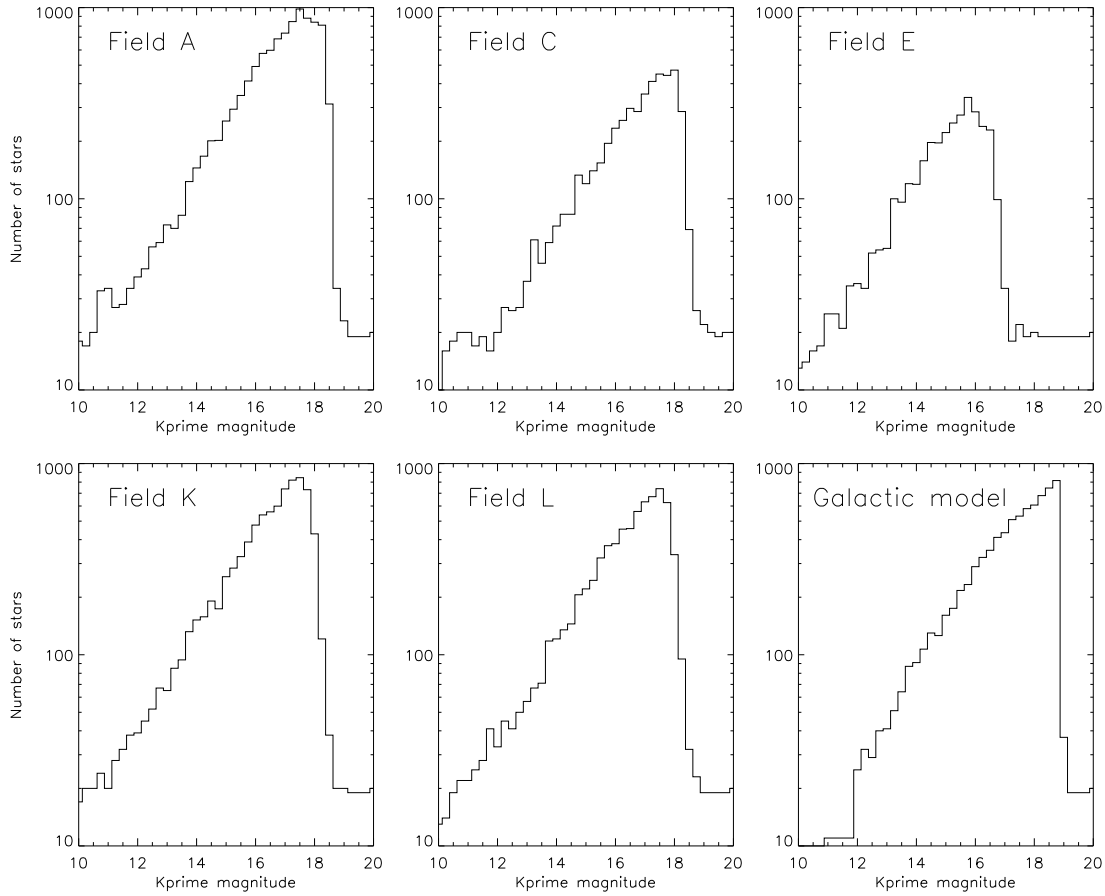
Figure 3.6: Completeness limits of the near-infrared wide-field survey. An histogram of the number of stars versus magnitude is shown for each individual optical field with K'-band observations. The completeness limits are 17.5 for fields A, C, K, and L and 15.5 for field E. The galactic model along the line of sight of the α Per cluster is displayed in the bottom right panel with an arbitrary cut at $K' = 19.0$ mag (Annie Robin, personal communication).

preferred to the Guide Star Catalogue (STScI, 2001) due to the better sky coverage and higher number of stars available in the α Per cluster.

We have, first, matched the pixel (x,y) coordinates to the celestial (ra,dec) coordinates of three reference stars chosen in the Omega-Prime field-of-view. The three stars were chosen to form a triangle which covers the largest area possible in the Omega-Prime frame. The reference stars should obviously not be aligned to provide a good first guess of the plate solution.

We have, then, extracted a plate solution from the three reference stars and refined it with stars common to the the USNO database and the Omega-Prime image (typically 50 to 100 stars), yielding accuracy of order 0.1–0.2″ in right ascension and declination.

Finally, we have updated the header of the fits file with the second-order polynomial fit for the plate solution, providing a file with pixel and celestial coordinates as well as photometry for each

individual source.

To check the validity of the plate solution, the science frames were displayed with the Skycat software and the USNO-A2 catalogue detections overplotted. The visualisation is straightforward since any discrepancy between the position of the USNO-A2 detections and the objects on the Omega-Prime images was immediately noticed.

3.5.4 Optical-infrared catalogue

As discussed extensively in Barrado y Navascués et al. (2002), near-infrared (JHK) follow-up observations of optically-selected cluster member candidates constitute good means to reject contaminating objects based on their location in various optical-infrared colour-magnitude diagrams. The infrared data were either extracted from the 2MASS database or obtained with Omega-Prime and Omega Cass on the Calar Alto 3.5-m telescope during various observing runs. Three subsamples were extracted and classified as follows:

- 54 are probable candidates

- 12 possible candidates

- 26 were rejected as cluster members

Some optically-selected cluster members were, however, lacking near-infrared information or had only upper limits. Furthermore, with a limiting magnitude of $K_s = 14.3$, the 2MASS survey provided near-infrared magnitudes only for objects at or above the stellar/substellar boundary in α Per. To estimate the contamination in the brown dwarf regime, deeper observations were therefore required. At the time of the observations, the full 2MASS database was not released, creating patches within the α Per cluster with no infrared data at all. Finally, another aim of the wide-field infrared survey was to uncover lower mass brown dwarfs down to the deuterium burning limit. Indeed, we have expected to find a near-infrared counterpart to faint object in the I_c-band (and no R_c measurement) in order to unveil new cluster brown dwarfs.

The cross-correlation of the optical (R_c and I_c) and near-infrared (K') catalogues was not straightforward. The matching radius was first increased to inspect the evolution of the number of matched objects with radii ranging from 0.1 to $10''$. The number of matches increased steeply up to 2–$3''$ and then kept rising slowly. To optimise the cross-correlation and avoid the loss of good candidates, we have estimated the dispersion in right ascension and declination between the optical and the near-infrared catalogues. The best gaussian fits to the distributions have sigma values of $0.372''$ and $0.193''$ for the right ascension and declination, respectively (Figure 3.7). The difference observed in the dispersion between both directions comes from the $\cos(\delta)$ not applied to the right ascension, especially at high declinations ($\delta = 48$–$50°$ for α Per). We have cross-correlated the near-infrared (K') and the optical (R_c and I_c) catalogues with matching radii of four times the dispersion values quoted above. Hence, we have missed only one or two objects among the 22,000 matches in the 0.70 square degree area surveyed in α Per.

The final catalogue is available upon request and will be available at the CDS website[2] after publication of the results of the infrared survey in α Per. The final catalogue contains 22,129

---

[2]http://vizier.u-strasbg.fr/cgi-bin/VizieR

entries with the right ascension and declination (in J2000), and the optical and near-infrared magnitudes. We will use this catalogue to extract the new cluster members in α Per and we will refer to these objects as new infrared-selected candidates as opposed to the optical members extracted by Barrado y Navascués et al. (2002). The selection procedure of the new candidates is described in the forthcoming sections.
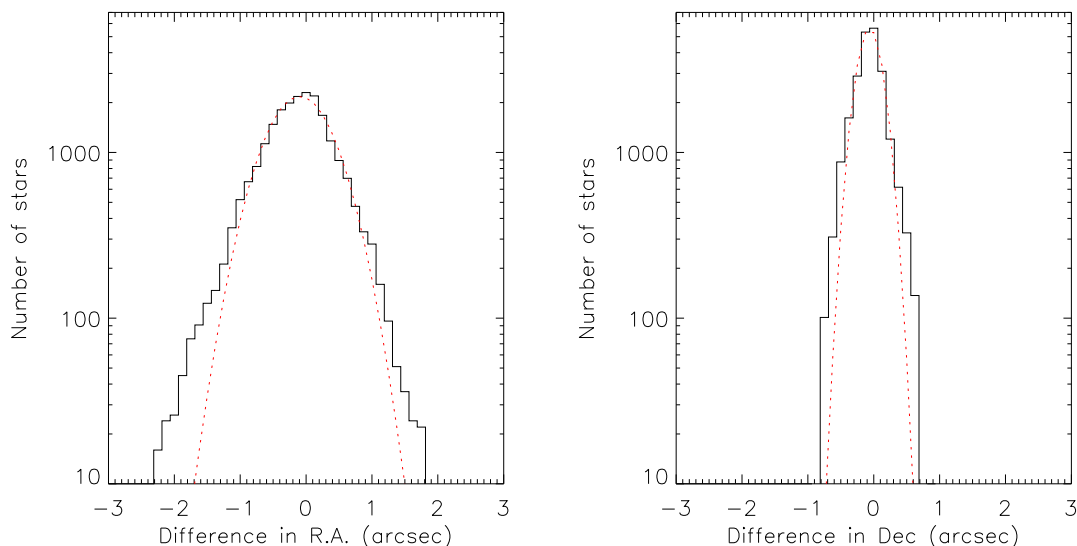

Figure 3.7: Determination of the matching radii in right ascension and declination for the cross-correlation of the optical and near-infrared catalogues of α Per. The left and right panel shows the number of stars versus the difference between the optical and the near-infrared coordinates in right ascension and declination, respectively. The histograms are shown for a matching radius of $10.0''$. The dotted curves represent the best gaussian fits to the distributions.

3.5.5 Colour-magnitude diagram

A colour-magnitude diagram represents the observational counterpart of the Hertzsprung-Russell diagram. The magnitudes on the y-axis correspond to the luminosities whereas the observed colours on the x-axis reflect the temperatures of the objects. Young cluster members will exhibit redder colours than their field counterparts and, therefore, occupy the right side of the plot.

The optical-to-infrared colour-magnitude diagram (K',I_c-K') is displayed in Figure 3.8. All sources detected within the 0.70 square degree area surveyed in the cluster are drawn as black dots. Overplotted are the NextGen isochrones (solid lines) for 50 and 100 Myr (Baraffe et al. 1998), the Dusty (dashed line), and Cond (dotted line) isochrones for 100 Myr (Chabrier et al. 2000b), assuming an age of 182 pc for the cluster. A reddening vector for $A_V = 2$ is also included for comparison purpose.

Three sequences are clearly visible in the (K',I_c-K') colour-magnitude diagram (Figure 3.8). The blue side of the diagram with $K \leq 18$ mag is populated by F and G dwarfs from the Galactic

thin disk, while fainter objects are F and G dwarfs belonging to the thick disk. Later-type K and M dwarfs populate the red side of the diagram. The bulk of objects seen on the right hand side below the isochrones with a I_c–K' colour of approximately 4 are mainly reddened background giants.
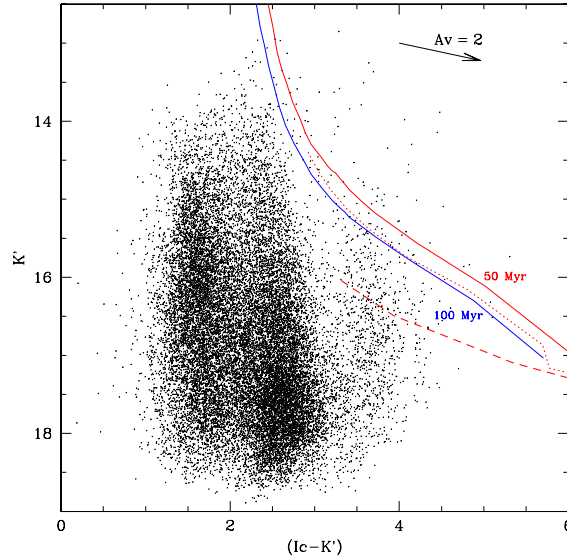

Figure 3.8: Colour-magnitude (K',I_c–K'). More than 22,000 detections over the 0.70 sq. deg. area surveyed in the α Per cluster are plotted as black dots. Also overplotted are the NextGen (solid lines) isochrones for 50 and 100 Myr (Baraffe et al. 1998), and Dusty (dashed line) 100 Myr isochrones (Chabrier et al. 2000b), assuming a distance of 182 pc for the cluster. A reddening vector for A$_V$ = 2 is also included for comparison purposes.

We have selected new member candidates from the optical-infrared survey of 0.70 square degree area in α Per by extracting objects falling to the right of the NextGen and Dusty 100 Myr isochrones (Figure 3.8 and Figure 3.9). As a first step, we have extracted all objects falling to the right of the NextGen 100 Myr isochrones over the whole magnitude range and assumed a distance of 182 pc for α Per. The total number of newly infrared-selected member candidates is 103 out of 22,129 detections in the 0.70 square degree surveyed area. Figure 3.9 provides a close-up region of the (K',I_c–K') colour-magnitude diagram where the new infrared-selected candidates are located. Those new cluster member candidates are represented by large hexagons and listed in the bottom panel of Table 3.2. We have also overplotted the optically-selected probable (filled triangles) and possible (open triangles) cluster member candidates from Barrado y Navascués et al. (2002) for comparison.

We have cross-correlated the new infrared-selected candidates with the recent release of the 2MASS database in order to provide additional J and H magnitudes. The K' magnitude from the wide-field survey and the K_s magnitudes from 2MASS are in good agreement. Analysis of the location of new candidates in various colour-magnitude diagrams confirmed their status as new probable cluster members, except for AP415 which appears redder in the optical (I_c,R_c–I_c) colour-magnitude diagram (Figure 3.3). This discrepancy might arise from a possible companion.

Further analysis of the membership status of the new cluster candidates will be pursued in the next section (§ 3.5.6).

In an attempt to estimate the influence of the distance on the candidate selection, we have repeated the procedure assuming distances of 176 pc and 190 pc, respectively. The number of infrared-selected candidates did vary as follows: 90 and 119 candidates were extracted for a distance of 176 and 190 pc, respectively. The additional objects found for a distance of 190 pc compared to 182 pc are included in Figure 3.9.

However, the NextGen isochrones do not include the modelling of dust in ultracool dwarfs. Several surveys in the field and in open clusters concluded that the spectral energy distributions of very low-mass stars and brown dwarfs are shaped by the presence of dust in their atmospheres.

We have, therefore, selected all objects located in the area delineated by the Dusty (masses below $50 \, M_{Jup}$ or T_{eff} below 2500 K) and the NextGen 100 Myr isochrones. Galactic models predict that those objects are mostly distant reddened giants but we would expect some cluster members hidden in this region of the colour-magnitude diagram. The number of selected objects are 269, 310, 333, assuming distances of 176, 182, and 190 pc, respectively. These numbers do not include the candidates selected based on the NextGen isochrones. All selection procedures assumed a mean extinction of 0.3 mag (Barrado y Navascués et al. 2002). The number of genuine cluster member candidates extracted from each selection method is given in the next section.

3.5.6 Colour-colour diagram

The colour-colour diagram is of prime importance to distinguish probable cluster member candidates from distant background giants. The photometry available in three broad-band filters (R_c, I_c, K') provides a colour-colour diagram $((I_c–K'),(R–I)_c)$ to further assess the membership of the infrared-selected candidates (Figure 3.10). The giant branch is clearly visible and centred approximately on $(R–I)_c \sim 1$ and $I_c–K' \sim 4$. Figure 3.10 displays all detections in the 0.7 square degree area surveyed in the α Per cluster (black dots) along with the NextGen 50 and 100 Myr isochrones (solid lines; Baraffe et al. 1998).

The initial selection of new cluster members using the NextGen 100 Myr isochrones at a distance of 182 pc for α Per extracted a total of 103 new infrared-selected candidates.

Among those new candidates, more than two-thirds of them (70 %) turned out to be reddened background giants (diagonal crosses on Figure 3.9 and Figure 3.11) rather than low-mass brown dwarf candidates, according to their location in the $((I_c–K'),(R–I)_c)$ colour-colour diagram. This contamination is caused by the ability of the K'-band to probe larger distances through highly extincted regions towards the Galactic plane, as it is the case for α Per.

The remaining infrared-selected candidates, which lie to the right of the NextGen 100 Myr isochrones in the colour-colour diagram, stay probable cluster member candidates. However, about half of these candidates (16 out of 30) were already extracted by the optical survey as probable members, thus, confirming their genuine membership. The shift in colour observed between the candidates and the isochrones originates from the selection procedure of these candidates and the uncertainties of the opacity line lists. We have recovered more than 50 % (18 out of 31) of the probable cluster members from Barrado y Navascués et al. (2002) (filled triangles in Figure 3.11 and upper panel in Table 3.2), distributed over the area surveyed in the near-infrared as follows.
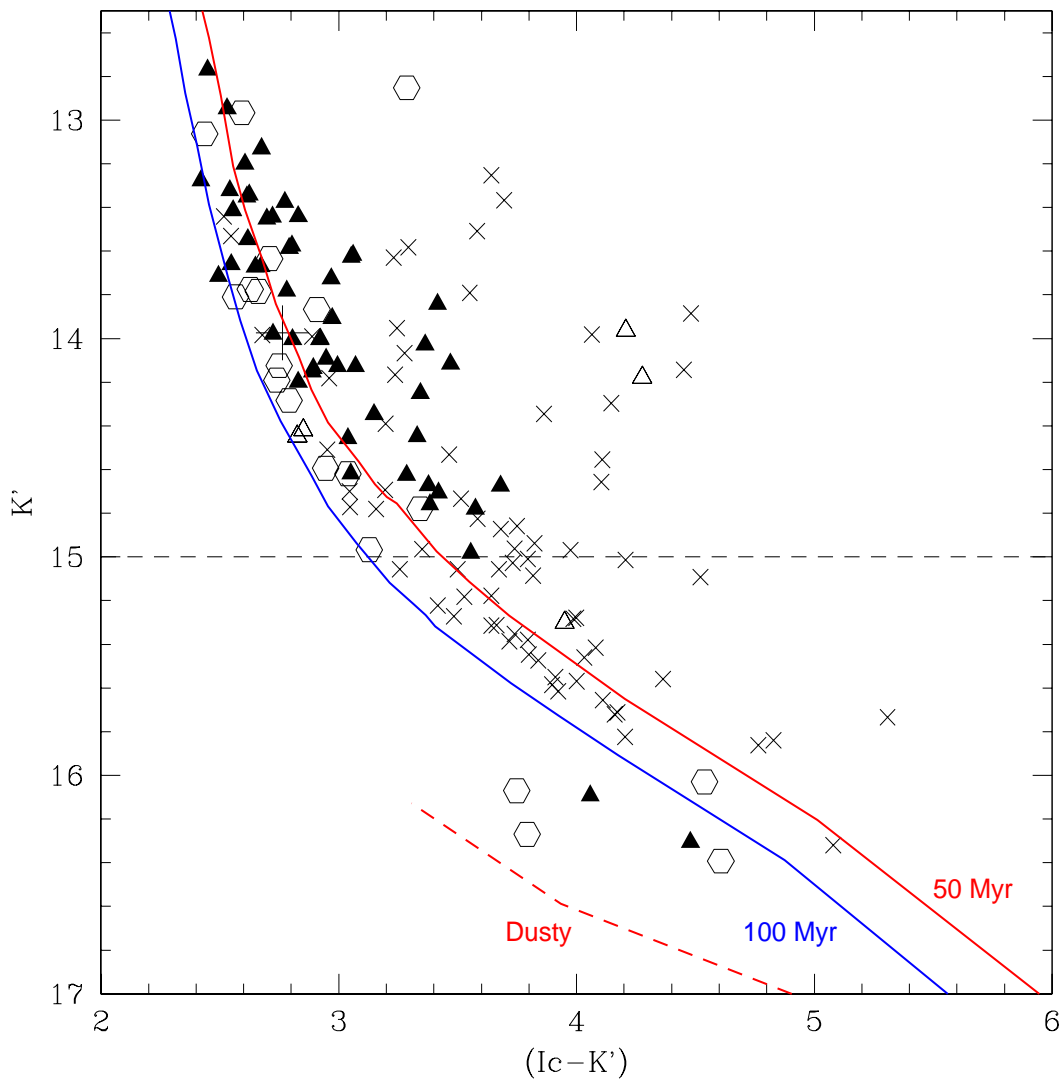
Figure 3.9: Colour-magnitude $(K', I_c - K')$ diagram showing the location of the new infrared-selected member candidates. Also overplotted are the NextGen (solid lines) isochrones for 50 and 100 Myr (Baraffe et al. 1998) and the Dusty (dashed line) 100 Myr isochrones (Chabrier et al. 2000b), assuming a distance of 182 pc for the cluster. Filled and open triangles are probable and possible cluster member candidates extracted by the optical survey described in Barrado y Navascués et al. (2002). Open hexagons are new infrared-selected cluster member candidates from our optical-infrared survey. The two selection methods are clearly apparent. The diagonal crosses indicate the distant background giants. The horizontal dashed line represents the stellar/substellar boundary at $M_K = 8.7$ mag ($M_I = 11.8$ mag) assuming a distance of 182 pc for the cluster.

Figure 3.10: Colour-colour ((I_c–K'),(R–$I)_c$). All 22,129 detections are plotted as black dots. Also overplotted are the NextGen (solid lines) isochrones for 50 and 100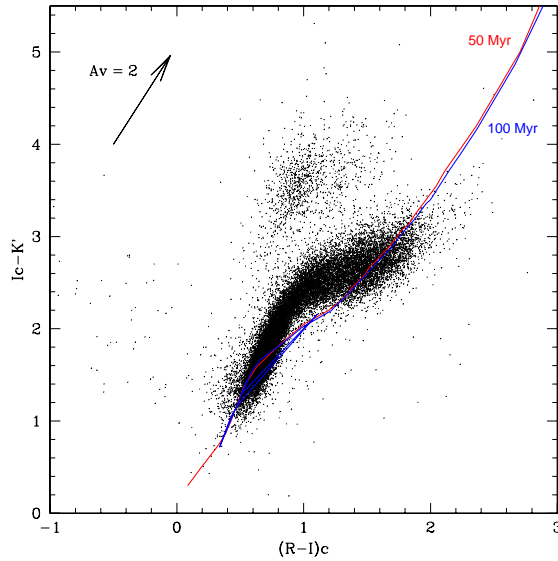 Myr (Baraffe et al. 1998), age bracketing the one estimated for α Persei, assuming a distance of 182 pc. The giant branch is well populated in this diagram ((R–$I)_c \sim 1$ and I_c–$K' \sim 4$), due to the low galactic latitude of the α Per cluster. A reddening vector for $A_V = 2$ is also included for comparison purpose.

- Three probable cluster members out of four in the field A

- Three out of six in field C

- Two out of three in field E

- Five out of seven in field K

- Five out of eleven in field L

The remaining 14 objects are new infrared-selected probable member candidates not extracted as such by the optical survey (open hexagons in Figure 3.11 and lower panel in Table 3.2). One of these new member candidates (AP426) has R_c, I_c, and K' magnitudes below the hydrogen-burning limit, indicating a probable brown dwarf cluster member. Another candidate (AP425) straddles the stellar/substellar boundary and is possibly a brown dwarf. Finally, AP424 lies close to the lithium depletion boundary estimated by Stauffer et al. (1999).

Moreover, one object, previously classified as a non-member by Barrado y Navascués et al. (2002), was included in our sample as well (large cross in Figure 3.11).

As mentioned earlier (§ 3.5.5), our selection of new cluster members in α Per to the right of the NextGen 100 Myr isochrones extracted 90 and 119 candidates for distances of 176 and 190 pc, respectively. How does the number of infrared-selected cluster member candidates and/or giants depend on the assumed distance?
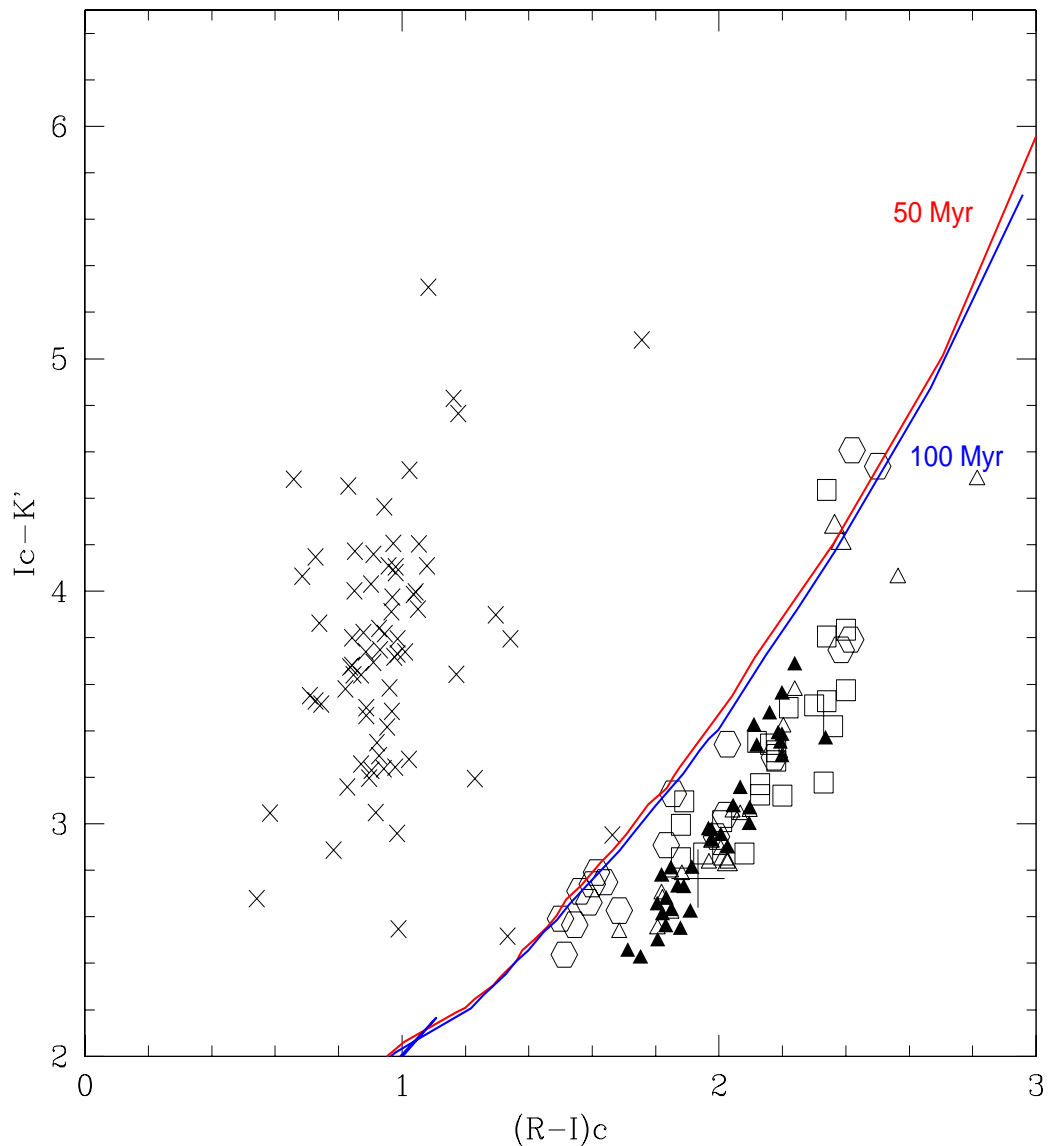
Figure 3.11: Colour-colour diagram $((I_c-K'),(R-I)_c)$. Also overplotted are NextGen (Baraffe et al. 1998) isochrones for 50 and 100 Myr, age bracketing the one estimated for the cluster. Filled and open triangles are probable and possible cluster member candidates extracted by the optical survey described in Barrado y Navascués et al. (2002). Open squares are spectroscopically confirmed members of α Per from Stauffer et al. (1999). Open hexagons are new infrared-selected cluster member candidates from our optical-infrared survey. The diagonal crosses indicate the distant background giants rejected as cluster member. The discrepancy between isochrones and cluster candidates might originate from the uncertainties on the current opacity line lists.

Table 3.2: List of the new member candidates of the α Per cluster selected from the optical-to-infrared survey (Section 3.5). The names, coordinates in J2000, and R_c, I_c, the 2MASS J, H, and K_s magnitudes and K' magnitudes from our near-infrared observations as well as the colours of each object are quoted. The upper part of the table provide the list of optically-selected member candidates found independently in the optical-to-infrared survey whereas the lower part lists the new infrared-selected probable candidates. Among them, four new objects are brown dwarf candidate members. The numbering of the new candidate members follows the one described in Barrado y Navascués et al. (2002) and stars at AP413.

Name	R.A.	Dec	R_c	I_c	J	H	Ks	K'	$(R–I)_c$	$(I_c–K')$
Optically-selected cluster member candidates										
AP329	03:23:56.36	+48:09:21.1	17.16	15.48	13.88	13.31	13.04	12.95	1.69	2.53
AP332	03:25:16.91	+48:36:09.3	17.63	15.80	14.06	13.43	13.19	13.13	1.82	2.67
AP334	03:22:45.51	+48:21:33.4	17.82	15.96	14.25	13.66	13.34	13.35	1.85	2.61
AP339	03:26:33.28	+50:07:41.9	17.97	16.15	14.35	13.76	13.40	13.45	1.82	2.70
AP343	03:23:48.49	+48:36:43.3	18.01	16.21	14.62	14.07	13.72	13.66	1.81	2.55
AP344	03:26:52.11	+50:00:32.8	18.24	16.27	14.33	13.69	13.39	13.44	1.97	2.83
AP309	03:22:40.69	+48:00:33.8	18.23	16.38	14.49	13.88	13.58	13.59	1.85	2.79
AP349	03:26:48.01	+50:02:15.7	18.45	16.56	14.62	14.04	13.73	13.78	1.88	2.78
AP353	03:24:48.69	+48:49:47.3	18.78	16.68	14.61	14.00	13.65	13.63	2.10	3.05
AP364	03:20:39.19	+49:32:06.2	18.90	16.92	15.00	14.41	14.03	14.00	1.98	2.92
AP365	03:28:22.98	+49:11:24.3	19.06	17.03	15.02	14.33	14.15	14.20	2.03	2.83
AP366	03:26:35.49	+49:15:44.2	19.05	17.04	15.12	14.54	14.22	14.15	2.00	2.89
AP369	03:26:45.11	+50:25:06.7	19.46	17.26	14.88	14.26	13.88	13.84	2.20	3.42
AP311	03:23:08.70	+48:04:50.7	19.56	17.50	15.44	14.71	14.32	14.46	2.07	3.04
AP370	03:27:01.00	+49:14:41.2	19.71	17.67	15.61	14.94	14.50	14.62	2.04	3.05
AP305	03:19:21.62	+49:23:31.1	20.59	18.36	15.81	14.96	14.64	14.78	2.24	3.57
AP399	03:25:48.55	+50:01:00.8	22.71	20.15	—	—	—	16.09	2.56	4.06
AP406	03:23:09.86	+48:16:30.0	23.60	20.78	—	—	—	16.31	2.81	4.48
New infrared-selected cluster member candidates(NextGen isochrones)										
AP413	03:24:17.75	+48:07:36.0	17.01	15.50	14.03	13.34	13.05	13.06	1.51	2.44
AP414	03:22:05.17	+48:12:46.1	17.06	15.56	14.00	13.26	13.05	12.97	1.50	2.59
AP415	03:25:32.89	+48:45:21.4	18.31	16.14	13.75	13.06	12.82	12.85	2.17	3.29
AP416	03:28:16.33	+50:05:51.6	17.91	16.34	14.57	13.91	13.63	13.63	1.56	2.71
AP417	03:22:40.50	+48:19:35.0	18.09	16.40	14.80	14.09	13.83	13.78	1.69	2.63
AP418	03:26:02.06	+50:05:34.7	18.04	16.45	14.68	14.06	13.71	13.78	1.59	2.66
AP419	03:23:18.80	+48:04:25.4	18.61	16.77	14.75	14.07	13.77	13.87	1.83	2.91
AP420	03:27:17.27	+50:07:19.8	18.51	16.87	15.12	14.41	14.13	14.12	1.64	2.75
AP421	03:22:09.83	+48:16:43.8	18.53	16.93	15.30	14.66	14.28	14.19	1.60	2.74
AP422	03:23:17.96	+47:59:01.7	18.69	17.07	15.31	14.54	14.20	14.28	1.61	2.79
AP423	03:24:08.12	+48:48:30.0	19.53	17.54	15.50	15.03	14.44	14.59	1.99	2.94
AP424	03:23:04.86	+48:16:11.3	19.68	17.66	14.61	15.15	14.61	14.62	2.02	3.04
AP425	03:27:07.06	+50:09:22.7	20.15	18.12	15.75	15.00	14.77	14.78	2.03	3.34
AP426	03:26:16.24	+50:18:43.3	23.07	20.57	—	—	—	16.03	2.50	4.54
AP427	03:23:59.92	+48:08:00.5	17.92	16.38	14.84	14.09	13.87	13.81	1.54	2.57
AP428	03:23:05.59	+48:09:00.7	19.95	18.10	16.12	15.07	14.76	14.97	1.85	3.13
New infrared-selected cluster member candidates(Dusty isochrones)										
AP429	03:27:30.59	+49:11:09.6	22.48	20.06	—	—	—	16.27	2.42	3.79
AP430	03:20:14.94	+49:31:46.6	23.42	21.00	—	—	—	16.39	2.42	4.61
AP331	03:24:06.45	+48:23:11.5	22.20	19.82	—	—	—	16.07	2.39	3.76

For a distance of 176 pc, the list of 90 candidates is divided as follows:

- 64 candidates (71 %) turned out to be giants.

- One object was previously classified as non-member by Barrado y Navascués et al. (2002).

- 15 candidates are common to the optical and near-infrared surveys.

- 10 are new infrared-selected candidates. The 'missing' new candidates compared to distance of 182 pc are AP421, AP422, AP423, and AP426, the latter being a possible cluster brown dwarf.

For a distance of 190 pc, the list of 119 candidates is divided as follows:

- 86 candidates (72 %) are classified as giants

- The same candidate classified as non-member by Barrado y Navascués et al. (2002).

- 16 objects are common candidates as for a distance of 182 pc

- 16 new candidates including two new ones, AP427 and AP428, represent our new infrared-selected candidates. AP428 is straddling the stellar/substellar boundary, indicating a possible brown dwarf member.

To summarise, the number of giants is approximately 70 % of all infrared-selected candidates. The number of new member candidates is 16, assuming the distance derived from isochrone fitting. However, all these new candidates are stellar components of the α Per cluster except, AP426.

To find new brown dwarf candidates in the cluster, we have examined the location in the colour-colour diagram of the objects selected to the right of the Dusty 100 Myr isochrone in the colour-magnitude diagram. Following the previous selection procedure, we could extract 5 new brown dwarf candidates, including the recovery two candidates from Barrado y Navascués et al. (2002). The latter two brown dwarfs, AP399 and AP406, were lacking near-infrared photometry. The numbering of the new candidates strictly follows the previous one and starts at AP439. The remainder objects, rejected as possible cluster members, are mostly distant reddened giants as anticipated by galactic models (not shown in Figure 3.11 to avoid overloading the plot).

One can now ask the following question: why were those new infrared-selected cluster member candidates missed in the optical selection? To address this issue, we have compared the location of the new candidates to previous members in the optical $(I_c,(R\text{--}I)_c)$ colour-magnitude diagram (Figure 3.3).

All the infrared-selected candidates located to the right of the NextGen isochrones in the $(K',I_c\text{--}K')$ colour-magnitude diagram also lie to the right of the NextGen isochrones in the $(I,R\text{--}I)$ colour-magnitude diagram. They define a bluer sequence than the probable members extracted by Barrado y Navascués et al. (2002) and remain, therefore, likely new cluster member candidates. Some objects follow the sequence defined by the probable candidates extracted by Barrado y Navascués et al. (2002). One object, AP415, lie above the sequence and might be either a contaminant or a binary belonging to the cluster (Figure 3.3). Optical spectroscopy is required to ascertain the membership of these new infrared-selected cluster members.

The new brown dwarf candidates follow the sequence defined by the probable candidates from Barrado y Navascués et al. (2002). The faintest new brown dwarf candidate, AP431, exhibit bluer optical colour which might reflect the settling of dust in the atmospheres of young substellar objects.

3.6 Optical spectroscopy of cluster member candidates

Due to the low galactic latitude of the α Per cluster, proper motion and photometry alone fail to eliminate all non-members. The membership of the new cluster member candidates extracted

by Barrado y Navascués et al. (2002) and our near-infrared wide-field survey are solely based on colour selection as no first epoch is available due to the faintness of the objects. To ascertain the membership of the photometrically-selected candidates in α Per, we were granted four observing nights in autumn 2002 to carry out moderate-resolution optical spectroscopy of the new candidates with the Twin spectrograph mounted on the Calar Alto 3.5-m telescope.

The spectroscopic observations are described in § 3.6.1. The data reduction is detailed § 3.6.2. The main results of the spectroscopy of the new cluster member candidates in α Per are presented in § 3.6.3.

3.6.1 Spectroscopic observations

Spectroscopic observations were conducted with the Twin spectrograph mounted on the Calar Alto 3.5-m telescope in October/November 2002 under variable weather conditions over the four night observing run.

The Twin CCD camera is a 2000×800 pixel detector with a spatial resolution of 0.5 Å/pixel. The light entering the spectrograph is separated by a dichroic beam splitter which allows the user to obtain a blue and red spectrum of the target. We have obtained moderate-resolution ($R \sim 2000$) optical spectra of 33 selected member candidates using the T07 grating covering 5800–8800 Å. Our sample of objects can be divided into four categories:

- 24 probable members (Barrado y Navascués et al. 2002)

- 1 possible member, AP350 (Barrado y Navascués et al. 2002)

- 4 non-members: AP327, AP336, AP338, and AP342 (Barrado y Navascués et al. 2002)

- Four new infrared-selected members: AP414, AP415, AP416, and AP418

We have observed most of the objects three times (Table 3.3), each exposure being shifted along the slit by approximately 100 pixels. Table 3.3 lists the 33 objects observed spectroscopically, their I_c magnitudes, the observing dates, the exposure times, as well as spectroscopic results which are detailed in the next section (§ 3.6.3). We have used two different slits ($1.5''$ and $2.1''$) depending on the seeing conditions. We have adjusted the exposure times taking into account the brightness of the object as well as the weather conditions. We have taken dome flat fields, dark frames and He–Ar arc lamps before the beginning of each night as well. We have observed spectrophotometric standard stars Feige 110 (Hamuy et al. 1992) and G191-B2B (Massey & Gronwall 1990) twice each during the night to flux calibrate the spectra. Meanwhile, we have observed some template objects with known spectral types with the same set-up to derive accurate spectral type classification and compare gravity-sensitive absorption features. The template objects and their spectral types are GJ251 (M3.5), LHS1417 (M4.0), LHS0168 (M5.0), LHS1326 (M6.0), LHS0248 (M6.5), bracketing our cluster targets in spectral types.

3.6.2 Data reduction

The data reduction was entirely accomplished within the IRAF environment (package *twodspec* and *onedspec*). Each step of the procedure used to extract a one-dimensional optical spectrum is described below. The dispersion axis of the spectra obtained with the Twin spectrograph are along the lines and the blue wavelength are the end of the x-axis.

Table 3.3: List of all 33 objects observed with the red channel of the T07 grating on the Twin spectrograph at the Calar Alto 3.5-m telescope. Names, coordinates (in J2000), I_c magnitudes, observing date and exposure times, equivalent widths for Hα at 6563 Å, equivalent widths for the KI and NaI doublets at 7665/7699 Å and 8183/8195 Å, respectively, are included in the table. Values obtained for three spectral indices, TiO5 (Reid et al. 1995), VO-a (Kirkpatrick et al. 1999b), and PC3 (Martín et al. 1999b) are given in columns 10, 11, and 12, respectively. Former and new membership status as well as the spectral types with an uncertainty of half a subclass are provided in columns 13 and 14. The objects are in decreasing order of I_c magnitude.

Target	R.A.	Dec	I_c	Obs. Date	ExpT	Hα	KI	NaI	TiO5	VO-a	PC3	Member	Sp. Type
AP327	03:20:31.74	49:39:59.6	15.06	01 Nov 02	3×600s	—	—	—	0.985 (M***)	1.984 (M***)	1.109 (M***)	N → N	Giant
AP329	03:23:56.34	48:09:21.0	15.48	31 Oct 02	1×1800s	-6.5	2.0/1.3	2.1/2.4	0.390 (M4.0)	2.001 (M4.8)	1.236 (M4.7)	Y+ → Y	M4.5±0.5
AP414	03:22:05.21	48:12:46.0	15.56	03 Nov 02	3×600s	—	1.9/1.7	0.4/1.2	0.518 (M2.6)	1.950 (M4.2)	1.086 (M3.7)	N	M3.5±0.5
AP330	03:34:15.60	49:58:48.0	15.66	31 Oct 02	2×1800s	-10.2	2.6/1.6	2.7/3.4	0.375 (M4.5)	1.975 (M4.5)	1.240 (M4.7)	Y+ → Y	M4.5±0.5
AP283	03:24:38.78	48:17:17.1	15.70	10 Oct 02	2×1200s	-4.2	2.3/1.6	2.4/2.8	0.386 (M4.0)	1.987 (M4.6)	1.232 (M4.7)	Y+ → Y	M4.5±0.5
AP331	03:32:05.90	50:05:55.0	15.73	31 Oct 02	3×900s	-7.9	2.2/2.6	2.7/1.8	0.341 (M4.5)	1.973 (M4.5)	1.299 (M5.1)	Y+ → Y	M4.5±0.5
AP332	03:25:16.90	48:36:09.0	15.80	31 Oct 02	3×800s	-8.2	2.8/1.9	3.3/2.5	0.319 (M4.8)	1.992 (M4.7)	1.307 (M5.2)	Y+ → Y	M4.5±0.5
AP333	03:25:13.55	50:27:33.0	15.86	31 Oct 02	3×800s	-5.7	3.2/2.7	2.7/3.4	0.380 (M4.1)	1.942 (M4.1)	1.316 (M5.2)	Y+ → Y	M4.5±0.5
AP335	03:28:52.96	50:19:25.9	15.97	01 Nov 02	3×1500s	-10.7	3.6/1.8	2.9/3.2	0.352 (M4.4)	1.994 (M4.7)	1.306 (M5.2)	Y+ → Y	M4.5±0.5
AP336	03:31:55.30	49:08:31.0	16.04	01 Nov 02	3×600s	—	—	—	0.972 (M***)	1.971 (M***)	1.088 (M***)	N → N	Giant
AP337	03:34:07.50	48:32:08.0	16.07	01 Nov 02	3×1200s	-7.9	2.5/2.3	2.5/2.3	0.295 (M5.0)	2.006 (M4.8)	1.341 (M5.4)	Y+ → Y	M5.0±0.5
AP338	03:24:52.65	48:46:12.8	16.07	02 Nov 02	3×600s	—	—	—	0.964 (M***)	1.940 (M***)	0.953 (M***)	N → N	Giant
AP415	03:25:32.90	48:45:20.8	16.14	03 Nov 02	3×750s	—	1.1/2.0	1.1/0.8	0.520 (M2.6)	1.980 (M4.5)	1.030 (M3.2)	N	M3.5±0.5
AP339	03:26:33.24	50:07:41.7	16.15	01 Nov 02	3×1200s	-6.5	2.6/1.6	3.6/3.3	0.337 (M4.6)	1.982 (M4.6)	1.340 (M5.4)	Y+ → Y	M5.0±0.5
AP340	03:21:34.85	48:16:28.7	16.16	01 Nov 02	3×900s	-3.8	5.4/4.6	3.6/4.3	0.276 (M5.2)	2.018 (M4.9)	1.390 (M5.7)	Y+ → Y	M5.0±0.5
AP341	03:31:03.39	50:24:41.6	16.16	01 Nov 02	3×750s	-10.7	3.1/2.1	3.0/3.0	0.276 (M5.2)	1.997 (M4.7)	1.376 (M5.6)	Y+ → Y	M5.0±0.5
AP344	03:26:52.00	50:00:33.0	16.27	01 Nov 02	3×600s	-10.6	3.4/2.3	3.1/3.1	0.254 (M5.5)	2.030 (M5.1)	1.392 (M5.7)	Y+ → Y	M5.5±0.5
AP345	03:33:45.80	50:08:53.0	16.30	01 Nov 02	3×600s	-9.9	2.4/1.5	2.7/3.2	0.313 (M4.8)	1.995 (M4.7)	1.372 (M5.6)	Y+ → Y	M5.0±0.5
AP346	03:21:30.06	48:49:23.2	16.32	01 Nov 02	3×600s	-8.3	2.7/2.1	2.5/3.5	0.327 (M4.7)	1.981 (M4.5)	1.381 (M5.6)	Y+ → Y	M5.0±0.5
AP416	03:28:16.28	50:05:51.7	16.34	02 Nov 02	3×1200s	-4.8	0.9/1.0	2.3/2.3	0.520 (M2.6)	1.989 (M4.6)	1.048 (M3.4)	N	M3.5±0.5
AP347	03:31:33.77	49:52:02.1	16.34	01 Nov 02	3×600s	-6.9	3.1/1.9	3.0/3.0	0.288 (M5.1)	1.962 (M4.4)	1.368 (M5.6)	Y+ → Y	M5.0±0.5
AP342	03:25:39.24	48:45:21.1	16.34	02 Nov 02	3×600s	—	—	—	0.958 (M***)	1.998 (M***)	1.043 (M***)	N → N	Giant
AP309	03:22:40.65	48:00:33.6	16.38	01 Nov 02	3×600s	-4.9	2.1/1.5	2.3/1.6	0.345 (M4.5)	2.021 (M5.0)	1.336 (M5.4)	Y+ → Y	M5.0±0.5
AP418	03:26:02.08	50:05:34.5	16.45	03 Nov 02	2×750s	—	—	—	0.979 (M***)	1.970 (M***)	0.871 (M***)	N	Giant
AP349	03:26:47.90	50:02:16.0	16.56	02 Nov 02	3×1200s	-9.6	2.4/2.2	3.3/3.4	0.293 (M5.0)	1.986 (M4.6)	1.373 (M5.6)	Y+ → Y	M5.5±0.5
AP350	03:32:06.80	49:25:23.0	16.57	03 Nov 02	1×750s	—	—	—	1.017 (M***)	1.996 (M***)	0.913 (M***)	Y? → N	Giant
AP351	03:28:47.80	50:02:01.0	16.64	02 Nov 02	3×1200s	-7.6	2.5/2.1	3.5/3.7	0.295 (M5.0)	2.041 (M5.2)	1.322 (M5.3)	Y+ → Y	M5.0±0.5
AP353	03:24:48.66	48:49:47.0	16.68	02 Nov 02	3×1200s	-9.2	3.6/2.9	3.0/3.1	0.228 (M5.7)	2.061 (M5.4)	1.476 (M6.2)	Y+ → Y	M6.0±0.5
AP354	03:27:31.64	48:53:23.3	16.69	02 Nov 02	3×1200s	-11.1	3.4/2.6	2.9/3.2	0.224 (M5.8)	2.069 (M5.5)	1.458 (M6.1)	Y+ → Y	M6.0±0.5
AP355	03:22:33.15	48:47:00.3	16.70	02 Nov 02	3×1200s	-9.2	2.9/2.7	3.3/3.7	0.297 (M5.0)	2.005 (M4.8)	1.344 (M5.4)	Y+ → Y	M5.0±0.5
AP363	03:24:00.33	47:55:29.7	16.88	02 Nov 02	3×1200s	-14.9	3.1/2.0	3.7/4.1	0.288 (M5.1)	1.992 (M4.7)	1.400 (M5.8)	Y+ → Y	M5.5±0.5
AP364	03:20:39.16	49:32:06.0	16.92	02 Nov 02	3×1200s	-8.2	2.4/2.8	3.9/4.3	0.430 (M3.6)	2.028 (M5.0)	1.390 (M5.7)	Y+ → Y	M5.5±0.5
AP366	03:26:35.50	49:15:43.8	17.04	02 Nov 02	3×1200s	-10.5	3.4/2.3	3.1/3.1	0.244 (M5.6)	1.987 (M4.6)	1.417 (M5.9)	Y+ → Y	M6.0±0.5

1. The first step consists in creating an averaged bias frame. Ten bias images were taken before the night and were averaged with a minmax rejection. The lowest and highest value of each pixel were, therefore, removed and the remainder averaged. The mean bias was then subtracted from the raw science image.

2. A large number of cosmic rays affected the longest exposures necessary to obtain sufficient signal-to-noise ratio for the faintest cluster member candidates. We have employed a program using the convolution with a Laplacian kernel (van Dokkum 2001)[3] to remove cosmic rays because none of the IRAF task was found efficient in this respect.

3. We have averaged the five dome flat-fields taken before the beginning of the night with a minmax rejection. To correct for the wavelength dependence of the flat-field, we have fit a high-order polynomial along the dispersion axis of the flat-field. Then, we have divided the bias-corrected science frame by the normalised response function of the flat-field.

4. We have estimated the sky background around the spectrum by choosing two intervals to the left and to the right of the spectrum along the dispersion axis. The resulting image was a two-dimensional sky-subtracted spectrum of the object.

5. The centre of the spectrum, the width of the aperture, and the intervals for sky subtraction were chosen interactively until a satisfactory result was achieved. Finally, we have fit the trace of the spectrum by a cubic spline to extract the one-dimensional spectrum of the target.

6. A linear fit of the wavelength as a function of the pixel number was achieved by identifying helium and neon lines. For the Twin spectrograph, the blue wavelength corresponds to high number pixels. Three or four good lines were initially selected to obtain a first guess of the linear fit. The fit was refined using a larger number of lines with positions available in the IRAF database. Any discrepant line was deleted to optimise the fit.

7. The linear fit of the wavelength as a function of the pixel was then used to assign the dispersion solution to the science target. The starting and ending wavelengths as well as the wavelength per pixel were computed and should obviously match the parameters provided in the user manual of the instrument.

8. The flux calibration of the science spectrum required observations of spectrophotometric standard stars. The flux of the calibrated spectra is expressed in $\mathrm{erg\,cm^{-2}\,s^{-1}\,\AA^{-1}}$. We have applied the same data reduction procedure to the standard stars and the science targets. However, two additional steps were required to correct for the non-uniform response of the detector over the whole wavelength range. First, the flux of the standard star was integrated over 50 Å-wide bandpasses and corrected for exposure time. Second, the sensitivity function of the detector as a function of wavelength was computed taking into account the extinction.

Then, we have applied the fit of the sensitivity function to the dispersion-corrected one-dimensional spectrum of the target. Finally, we converted the spectrum into an ascii file with flux versus wavelength for further analysis. We have normalised the spectra at 7500 Å. Figure 3.12 displays *only* the objects whose spectroscopic results confirmed their status of bona-fide cluster member candidates.

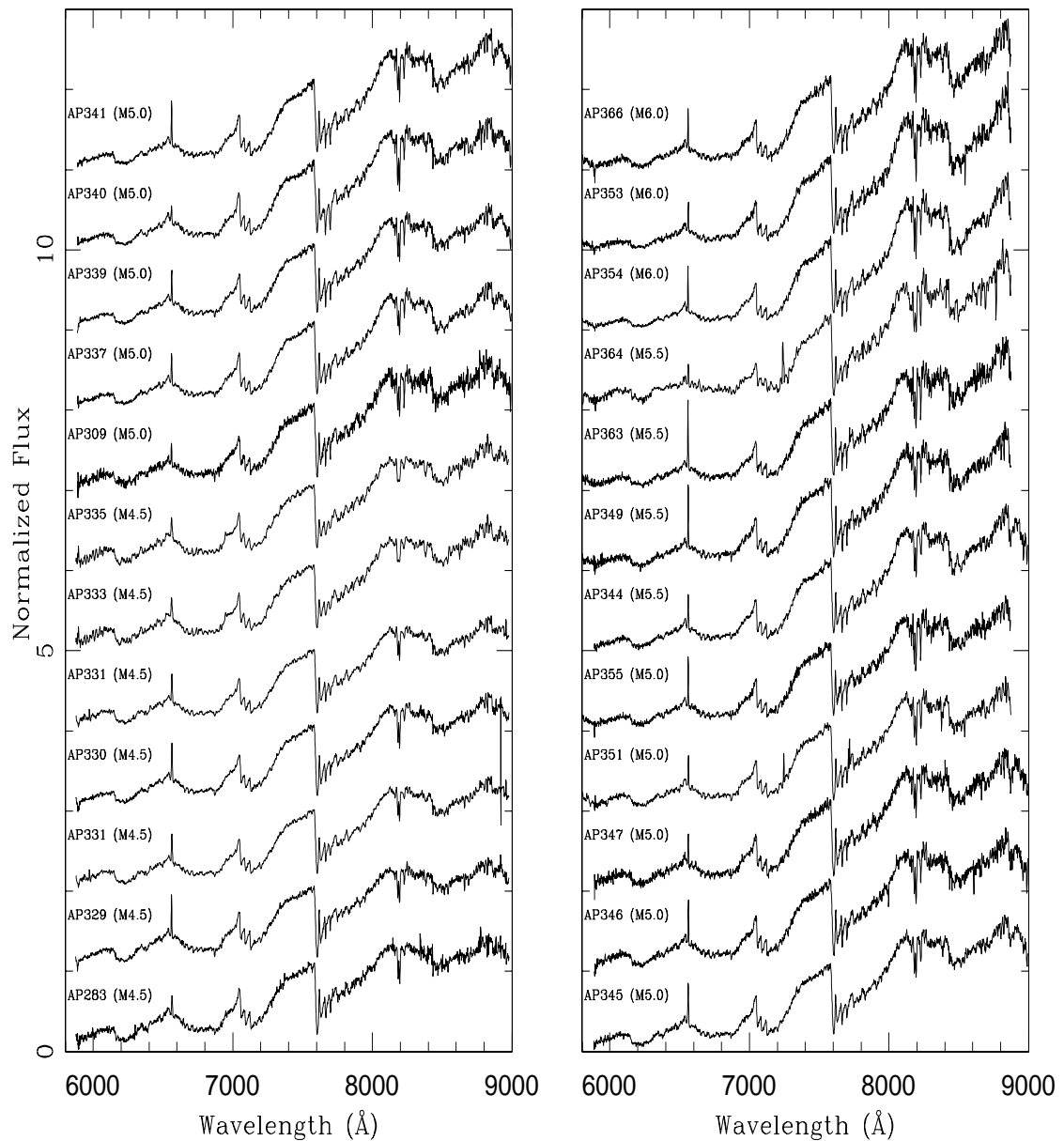[3]http://www.astro.yale.edu/dokkum/lacosmic/

Figure 3.12: Spectra of the 24 objects listed in Table 3.3 apart from the giants classified as a non-member and the new infrared-selected objects. The spectral types quoted into brackets after the name of the target range from M4.5 to M6.0 with a typical uncertainty of order half a subclass. Typical features of M dwarfs are clearly seen on the spectra, including TiO and VO absorption broad bands. All targets exhibit Hα in emission at 6563 Å. An arbitrary constant has been added to each spectrum for clarity.

3.6.3   Analysis of the optical spectra

We have observed spectroscopically a subsample of cluster member candidates in α Per containing 24 probable members, 1 possible member, and 4 non-members taken from the candidate list in Barrado y Navascués et al. (2002). The objects are listed in Table 3.3 along with their spectroscopic results. We have obtained optical (5800–8800 Å) spectroscopy with the Twin spectrograph of *all* probable members spanning $I = 15.0$–17.0, but four. Among the remaining four objects, we have taken optical spectra of two of them with the Keck telescope. Additionally, we have also carried out optical spectroscopy of *all* probable members spanning $I = 17.0$–18.0 with Keck. We will focus here on the optical spectroscopy conducted with the Twin spectrograph, including the nine candidates (AP329, AP332, AP309, AP339, AP349, AP344, AP353, AP364, and AP366) common to the near-infrared survey.

We have assigned a spectral type to each individual confirmed member with an uncertainty of half a subclass, according to the M dwarf classification schemes defined by Kirkpatrick et al. (1999b) and Martín et al. (1999b). The spectra of the non-members are consistent with giant spectra, confirming that these objects do not belong to the cluster. The only possible member candidate observed in the sample exhibits a similar spectrum and was, therefore, rejected as cluster member.

We have applied the "recipe" presented in § 1.4 to classify each probable cluster member. We have computed spectral indices for each individual target (Table 3.3), including TiO5 (Reid et al. 1995), VO-a (Kirkpatrick et al. 1999b), and PC3 (Martín et al. 1999b)[4].

The inferred spectral types from each index were generally consistent within a subclass. However, we have noticed some differences and favoured the direct comparison with spectral templates of well-known M dwarfs. The spectral indices quoted above were defined to classify field dwarfs which have larger gravity than young cluster members in α Per.

To derive a self-consistent classification and not rely solely on spectral indices, we have compared each individual target with spectra of template M dwarfs of similar spectral types, including 2MASS J2300189+121024, 2MASS J0244463+153531A&B, and 2MASS J0242252+134313 (Kirkpatrick et al. 1999b), as well as 2MASS J0435490+153720 (Gizis & Reid 1999), with spectral types M4.5, M5.0, M5.5, M6.5, and M6.0, respectively. In addition, due to possible differences in telescope/instrument configurations and detector sensitivities, we have observed comparison objects with known spectral types, including GJ251 (M3.0), LHS1417 (M4.0), LHS0168 (M5.0), LHS1326 (M6.0), and LHS0248 (M6.5) with the same instrument set-up. The three different spectral type estimates yielded consistent results with uncertainties of half a subclass (last column in Table 3.3 and Figure 3.12).

Finally, Table 3.3 shows that the brighter the cluster members are, the earlier is the spectral type. Furthermore, we have found the flux measured in the spectra of the targets consistent with the I_c magnitudes from the wide-field optical survey.

The objects displayed in Figure 3.12 span spectral types M4–M6, M6.5 being considered as the stellar/substellar border in young open clusters. All probable members in α Per, followed-up spectroscopically, are, therefore, stellar components of the cluster. According to the NextGen isochrones (Baraffe et al. 1998), the cluster members have masses ranging from $0.40\,\mathrm{M_\odot}$ to $0.12\,\mathrm{M_\odot}$, assuming a distance of 182 pc and an age of 90 Myr for α Per.

---

[4]The definition of the three spectral indices is given in Chapter 1 in Table 1.2

The Hα emission line at 6563 Å constitutes a further criterion to ascertain the membership of the selected cluster candidates as it is a sign of youth. This feature is clearly detected in *all* 24 probable candidates from Barrado y Navascués et al. (2002) (Figure 3.12). The Hα equivalent widths range from 4.0 to 15.0 Å and are consistent with previous measurements in α Per obtained by Zapatero Osorio et al. (1996), Prosser (1992, 1994), and Stauffer et al. (1999) in the M3–M6 spectral type range. However, the sample contains too few objects to probe the turnover around M3–M4 in α Per (Zapatero Osorio et al. 1996) caused by the transition from radiative to convective cores occurring at 0.3–0.2 $M_\odot$, regardless of the age (D'Antona & Mazzitelli 1994). This turnover was detected in the Pleiades cluster as well (Stauffer et al. 1994b; Hodgkin et al. 1995). Figure 3.13 shows Hα equivalent widths versus spectral types for previous α Per members (open triangles) and from our spectroscopy (filled hexagons).
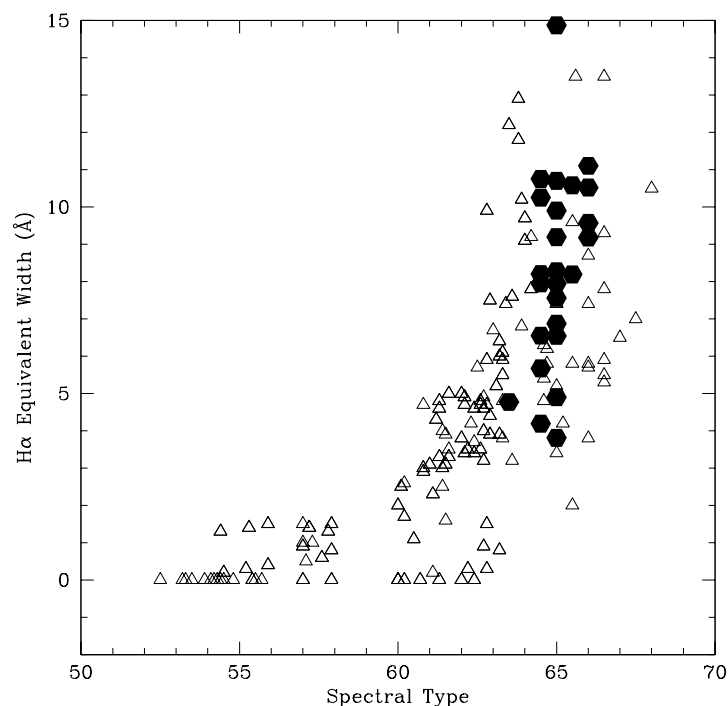

Figure 3.13: Hα equivalent widths versus spectral type for all spectroscopically confirmed cluster members in the α Per cluster. Open triangles indicate members listed in Prosser (1992, 1994) and Stauffer et al. (1999). Our Hα equivalent widths are indicated with filled hexagons and are consistent with measurements of cluster members with comparable spectral types. Values of 50, 60, and 70 given on the x-axis correspond to K0, M0, and L0 spectral types, respectively.

Furthermore, the strength of the Hα emission line in the α Per member candidates is stronger than in field dwarfs of similar spectral types although the chromospheric activity in field M dwarfs reaches a maximum around M6–M7 (Hawley, Gizis, & Reid 1996) and can be as high as in young magnetically active objects (Gizis, Reid, & Hawley 2002). We have compared the Hα equivalent widths of α Per cluster members to field M dwarfs of comparable spectral types extracted from

our sample of proper motion candidates (§ 2.4). Optical spectroscopy for field M dwarfs spanning M4–M6 shows that about half of them exhibit Hα with equivalent widths as large as those detected in α Per members.

Moreover, Hα equivalent widths measured in proper motion M4-M8 cluster members in the Pleiades is typically greater than 3 Å. Although arbitrary, the 3 Å value reflects the envelope of equivalent widths in the Pleiades (Hodgkin et al. 1995).

The detection of the Hα emission line in all probable cluster member candidates as well as the arguments presented here add support to the belief that there are indeed members of the cluster.

To further constrain the membership of the photometrically-selected candidates, we have computed the strengths of gravity-sensitive features, including the K I and Na I doublets at 7665/7699 Å and 8183/8195 Å, respectively (task *splot* in IRAF; Table 3.3). Young pre-main-sequence candidates are younger than field dwarfs and should, therefore, exhibit lower gravity. The equivalent widths of the gravity features Na I and K I versus spectral types are shown in Figure 3.14 for all probable member candidates observed spectroscopically.
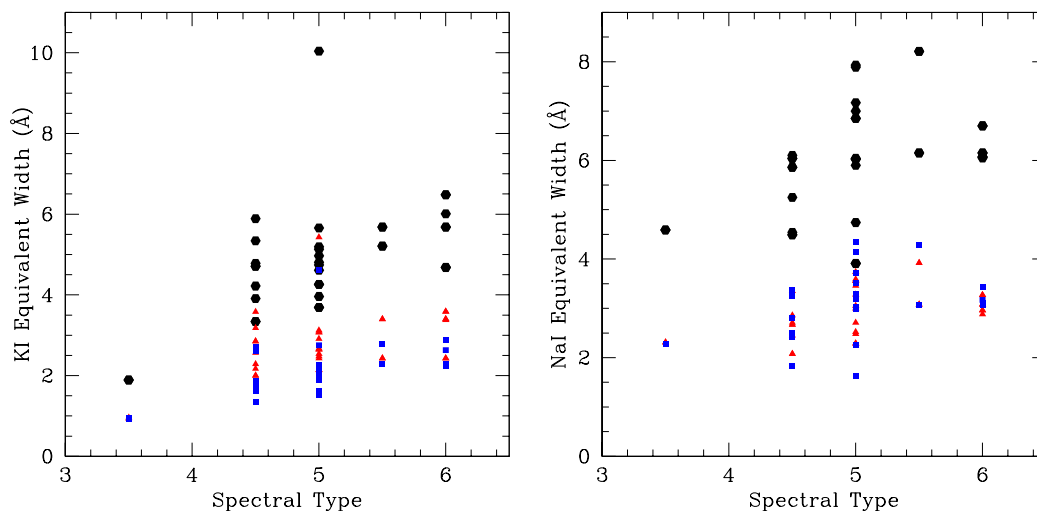

Figure 3.14: Equivalent widths (in Å) of gravity-sensitive absorption doublets (K I at 7665/7699 Å on the left panel and Na I at 8183/8195 Å on the right panel) for all spectroscopically confirmed cluster member in the α Per cluster. The hexagons indicate the sum of the equivalent widths of both lines whereas the triangles and the squares indicate the equivalent widths of the first and second line, respectively. Values of 3, 4, 5, and 6 on the x-axis correspond to spectral types of M3, M4, M5, and M6, respectively.

The equivalent width of the first absorption line of the K I doublet exhibit stronger equivalent widths than the second line while this trend is not obvious for the Na I doublet (Figure 2.4). Those measurements are comparable to results for the sample of field M dwarfs in the proper motion survey (Figure 2.4). The equivalent widths of the K I doublet in α Per are slightly smaller than for field M dwarfs of similar spectral types. Similarly, a difference in the Na I doublet equivalent widths between α Per and field dwarfs is observed when comparing Figure 2.4 and Figure 3.14

(note the difference in the Y-axis scale), indicative of a younger age. The differences are nevertheless small and might simply reflect the fact that the gravity difference in 100 Myr-old cluster members and old (1–5 Gyr) field dwarfs is less than 0.2 dex, according to the NextGen models (Baraffe et al. 1998). Our results regarding the equivalent widths of the Na I doublet are consistent with a total equivalent width of order 6 Å measured in the Pleiades (Martín et al. 1996). Our measurements are also larger than those in σ Orionis (Béjar et al. 1999).

As a whole, gravity measurements add support to the belief that those objects are genuine members of the α Per cluster.

The detection of the lithium absorption at 6708 Å is not expected as all candidates observed spectroscopically are stellar members of α Per.

We have obtained optical spectroscopy of a subsample of four infrared-selected member candidates in α Per (AP414, AP415, AP416, and AP418) to test the optical-to-infrared selection method presented in § 3.5. We have classified those objects according to their spectra as follows:

- One object (AP418) is clearly a non-member of the cluster due to its spectra exhibiting Hα and NaID in absorption as well as a proper motion inconsistent with the α Per cluster.

- We rejected two other candidates, AP414 and AP415, as possible members due to the non-detection of the Hα emission line and fluxes inconsistent with membership. They are likely contaminating field dwarfs with a spectral type of M3.5 ± 0.5.

- The last object, AP416, exhibits Hα although with an equivalent width weaker than those measured for the cluster members, but still consistent with previous studies in the α Per cluster (Figure 3.13). However, we would consider this object as a non-member because the spectral type (M3.5) is inconsistent with the measured I_c magnitude (Table 3.3).

To summarise, the fact that the four infrared-selected cluster member candidates in α Per are likely contaminating field dwarfs do not add strong support to the efficiency of the optical-to-infrared selection method in selecting cluster member candidates in a low galactic latitude open cluster as α Per.

The spectroscopy of the optically-selected candidates confirmed their membership. The probable candidates *all* exhibit Hα and have fluxes consistent with their spectral types. The previously classified non-members are, indeed, non-members as is the only possible members observed spectroscopically. Hence, the optical survey and the additional near-infrared imaging appear as excellent discriminant between cluster members and contaminants.

On the contrary, the optical-infrared survey alone appears less adequate at selecting cluster members as the contamination among selected objects is higher than in the optical. The large majority of candidates selected from the (K',I_c–K') colour-magnitude diagram are reddened background giants ($\sim 70\,\%$). Half of the remainder were previously considered as probable members while the rest awaits for spectroscopic follow-up observations. As a whole, the contamination lies in the range 70–85 %, twice larger than the optical selection (28–40 %; Barrado y Navascués et al. 2002). Despite the low statistics among infrared-selected cluster members with spectroscopic follow-up, none of the new candidates are bona-fide cluster members. We strongly emphasise the use of the K'-band as a tool to constrain the optical selection. However, one should be cautious using the optical-infrared (K',I_c–K') colour-magnitude diagram as a prime and sole criterion to

extract cluster members, in agreement with the Pleiades surveys focusing on deep optical surveys (R, I, and Z) to search for very low-mass stars and brown dwarfs. This procedure avoids large optical-to-infrared colours such as $I-K$, where reddened field dwarfs and distant background giants exhibit similar colours as young pre-main sequence stars.

3.7   Comparison of the α Per IMF with other open clusters

The new results from the optical spectroscopy of all probable members spanning $I_c = 15.0$–17.0 have confirmed their cluster membership status. Thus, we are in a position to assert that the mass function derived for the probable cluster members in α Per (bottom IMF in Figure 3.5) is the true cluster mass function according to our spectroscopic study. Despite the small number of possible members and non-members followed-up spectroscopically (5 objects out 38 extracted by the optical survey), those objects exhibit spectra inconsistent with cluster membership. These results were expected with regard to objects classified as non-members but the question remained open for the possible members. To summarise, the slope of the α Per open cluster remains $\alpha = 0.59 \pm 0.05$ (when expressed as the mass spectrum) in the 0.30–0.05 $M_\odot$ mass range where the photometric data are complete.

The Pleiades is the best studied young open cluster with a large number of photometrically-selected candidates being confirmed spectroscopically. Although most estimates of the index of the Pleiades mass function are not derived from an homogeneous and complete sample of spectroscopic members, power law indices (when expressed as the mass spectrum) agree within the uncertainties. Martín et al. (1998) derived $\alpha = 1.0 \pm 0.5$ in the 0.40–0.045 $M_\odot$ mass range based on a deep survey initiated by Zapatero Osorio et al. (1997b). Tej et al. (2002) estimated $\alpha = 0.5 \pm 0.2$ from 0.50 to 0.055 $M_\odot$ based on a pure statistical approach involving 2MASS and GSC databases. Dobbie et al. (2002) derived $\alpha = 0.8 \pm 0.2$ based on a deep optical photometric survey down to 0.040 $M_\odot$. Finally, Moraux et al. (2003) inferred $\alpha = 0.60 \pm 0.11$ over the 0.48–0.03 $M_\odot$ mass range from a deep (I, Z) survey complementing the (R, I) survey by Bouvier et al. (1998).

All the results from the Pleiades indicate an α index spanning 0.5–1.0 between 0.5 and 0.030 solar masses, in close agreement with the α Per estimate. Similar results are found in the Trapezium Cluster (Muench et al. 2002), in IC348 (Luhman et al. 2000), and in σ Orionis (Béjar et al. 2001), suggesting that the shape of the mass function in this mass range holds from few Myr up to few hundreds of Myr.

3.8   Conclusions on α Per and future plans

We have carried out a wide-field near-infrared (K'-band) survey of a 0.70 square degree area in the α Per cluster. Combining the new infrared photometry with existing optical (R_c and I_c) imaging, we have extracted a total of 198 new cluster member candidates based on their location in the optical-to-infrared (K',I_c-K') colour-magnitude diagram. However, the position of these new candidates in the colour-colour diagram revealed that about 80 % of them are contaminants, including reddened field dwarfs and a large number of background giants due to the low galactic latitude of the cluster. The optical (I_c,($R-I$)$_c$) colour-magnitude diagram shows that the new infrared-selected candidates define a bluer sequence than previous probable members in α Per but remain bona-fide cluster members. Among the new candidates, we have unveiled four new brown

dwarf candidates.

Additional optical (5800–8800 Å) spectroscopy of four infrared-selected cluster member candidates has revealed that their spectral types and $H\alpha$ equivalent widths are inconsistent with cluster membership. About 40 new infrared-selected remain as probable cluster members, including 18 objects already classified as such by Barrado y Navascués et al. (2002). Their optical and optical-to-infrared colours are consistent with membership but spectroscopic confirmation is lacking.

We have also presented moderate-resolution (R $\sim$ 2000) optical (5800–8800 Å) spectroscopy of 29 candidates extracted by Barrado y Navascués et al. (2002) with the Twin spectrograph mounted on the Calar Alto 3.5-m telescope. The sample contains twenty-four probable cluster member candidates, one possible member, and the remainder were classified as non-members. All probable members have spectral types, Hα equivalent widths, and gravity measurements consistent with cluster membership. The other candidates are clearly non-members with respect to their spectra. All probable members spanning $I_c = 15.0$–17.0 in α Per, but four, have been spectroscopically followed-up. Their spectral types range from M4 to M6 and their masses from 0.40 to $0.12\,M_\odot$.

The α Per mass function is, therefore, well represented by the probable mass function derived by Barrado y Navascués et al. (2002) and approximated by a power law with a slope of 0.59 over the 0.30–$0.05\,M_\odot$ mass range, when expressed as the power spectrum. This mass function is confirmed down to $0.12\,M_\odot$ with our results based on *photometric and spectroscopic* membership criteria.

The optical spectroscopy has demonstrated that the optical (R and I) photometry with near-infrared follow-up imaging constitutes a good discriminant between field stars and young cluster members. More recently, deep (I and Z) surveys have proven very efficient to detect lower mass brown dwarfs in open clusters due to the saturation of the R–I colours at late spectral types.

The near-infrared wide-field survey combined with existing optical photometry is hampered by higher contamination by background objects than purely optical surveys. A combination of optical and near-infrared imaging is nevertheless mandatory to disentangle cluster members from contaminants.

We would like to stress here some issues related to the future deep near-infrared surveys planned within the framework of the UKIDSS and CFHT consortia. Both surveys aim at surveying large area in well-known open clusters, including α Per. On the one hand, such deep surveys are required to supersede the 2MASS database and enable cross-correlation with faint objects unveiled in on-going deep optical surveys. On the other hand, these surveys would be optimised by including one (or two) optical filters to reveal less massive brown dwarfs in clusters. Near-infrared surveys remain, however, extremely efficient in star-forming regions where the high extinction hampers optical observations.